

The Full $B \rightarrow D^* \tau^- \bar{\nu}_\tau$ Angular Distribution and CP violating Triple Products

Murugeswaran Duraisamy^a and Alakabha Datta^a

^a *Department of Physics and Astronomy, 108 Lewis Hall,*

University of Mississippi, Oxford, MS 38677-1848, USA

E-mail: duraism@phy.olemiss.edu, datta@phy.olemiss.edu

ABSTRACT: We perform a comprehensive study of the impact of new-physics operators with different Lorentz structures on $\bar{B} \rightarrow D^{*+} l^- \bar{\nu}_l$ decays, ($l = e, \mu, \tau$) involving the $b \rightarrow cl\nu_l$ transition. We present the full three angle and q^2 angular distribution with new physics operators with complex couplings. Various observables are constructed from the angular distribution with special focus on the CP violating triple product asymmetries which vanish in the Standard Model without any hadronic complications. Two of the three triple products are only sensitive to vector/axial vector new physics operators. Hence, the measurements of non-zero triple-product asymmetries will be a clear sign of new physics and a strong signal for vector/axial vector new physics operators. Even though we focus on τ final state, one can use the triple-products to search for new physics with e and μ in the final state.

KEYWORDS: B Physics, Beyond Standard Model.

Contents

1. Introduction	1
2. Formalism	3
2.1 Constraints on the NP couplings	6
3. Angular analysis	8
3.1 Differential branching ratio	10
3.2 Polarization fraction for D^*	12
3.3 Distribution in $\cos\theta_l$ and A_{FB}	12
3.4 Asymmetries $\mathbf{A}_C^{(i)}$ in the angular variable χ	14
3.4.1 $A_C^{(1)}$	15
3.4.2 $A_C^{(2)}$	15
3.4.3 $A_C^{(3)}$	17
3.5 CP-violating triple-product asymmetries	18
3.5.1 $A_T^{(1)}$	19
3.5.2 $A_T^{(2)}$	20
3.5.3 $A_T^{(3)}$	21
3.6 Correlations between R_{D^*} and q^2 -integrated TP asymmetries	22
4. Discussion and Summary	24
A. Details of the $\bar{B} \rightarrow D^* \tau^- \bar{\nu}_\tau$ angular analysis	26
A.1 kinematics	26
A.2 Form Factors	27
B. Form factors in the Heavy Quark Effective Theory	27
B.1 Angular coefficients	28

1. Introduction

The Standard Model (SM) of particle physics, even though very successful, is expected to break down at some energy scale and make way for a more complete theory. Exploration of what lies beyond the SM can be carried out at the energy frontier in colliders such as the LHC or at the intensity frontier at high luminosity

experiments. In the intensity frontier, the B factories, BaBar and Belle, have produced an enormous quantity of data in the last decade. There is still a lot of data to be analyzed from both experiments. The B factories have firmly established the CKM mechanism as the leading order contributor to CP violating phenomena in the flavor sector involving quarks. New physics (NP) effects can add to the leading order term producing deviations from the SM predictions. In this respect, the second and third generation quarks and leptons are quite special because they are comparatively heavier and are expected to be relatively more sensitive to NP. As an example, in certain versions of the two Higgs doublet models (2HDM), the couplings of the new Higgs bosons are proportional to the masses and so NP effects are more pronounced for the heavier generations. Moreover, the constraints on NP involving the third generation leptons and quarks are somewhat weaker allowing for larger NP effects.

It is interesting that there are certain discrepancies in decays involving τ and ν_τ states, though none of them are significant enough to establish clearly the presence of NP. There is a seeming violation of universality in the tau lepton coupling to the W suggested by the Lep II data which could indicate NP associated with the third generation lepton [1]. Recent measurement of CP violation [2] in τ decays find A_{CP} in $\tau^- \rightarrow \pi^- K_s(\geq 0\pi^0)\nu_\tau$ is $(-0.36 \pm 0.23 \pm 0.11) \%$ which is different from the SM prediction (0.36 ± 0.01) by 2.8σ . The branching ratio of $B \rightarrow \tau\nu_\tau$ showed some tension with the SM predictions [3] indicating NP, possibly coming from an extended scalar or gauge sector [4]. However, new Belle [5] and BaBar [6] measurements, obtained using the hadronic tagging method, are more consistent with the SM.

If there is NP involving the third generation leptons one can search for it in semileptonic $b \rightarrow c\tau\nu_\tau$ decays such as $\bar{B} \rightarrow D^+\tau^-\bar{\nu}_\tau$, $\bar{B} \rightarrow D^{*+}\tau^-\bar{\nu}_\tau$ [7]. The semileptonic decays of B meson to the τ lepton is mediated by a W boson in the SM and it is quite well understood theoretically. In many models of NP this decay gets contributions from additional states like new vector bosons or new scalar particles. The exclusive decays $\bar{B} \rightarrow D^+\tau^-\bar{\nu}_\tau$ and $\bar{B} \rightarrow D^{*+}\tau^-\bar{\nu}_\tau$ are important places to look for NP because, being three-body decays, they offer a host of observables in the angular distributions of the final state particles. The theoretical uncertainties of the SM predictions have gone down significantly in recent years because of the developments in heavy-quark effective theory (HQET). The experimental situation has also improved a lot since the first observation of the decay $\bar{B} \rightarrow D^{*+}\tau^-\bar{\nu}_\tau$ in 2007 by the Belle Collaboration [8]. After 2007 many improved measurements have been reported by both the BaBar and Belle collaborations and the evidence for the decay $\bar{B} \rightarrow D^+\tau^-\bar{\nu}_\tau$ has also been found [9, 10, 11]. Recently, the BaBar collaboration with their full data sample of an integrated luminosity of 426 fb^{-1} has reported the

measurements of the quantities [12]

$$\begin{aligned}
R(D) &= \frac{BR(\bar{B} \rightarrow D^+ \tau^- \bar{\nu}_\tau)}{BR(\bar{B} \rightarrow D^+ \ell^- \bar{\nu}_\ell)} = 0.440 \pm 0.058 \pm 0.042, \\
R(D^*) &= \frac{BR(\bar{B} \rightarrow D^{*+} \tau^- \bar{\nu}_\tau)}{BR(\bar{B} \rightarrow D^{*+} \ell^- \bar{\nu}_\ell)} = 0.332 \pm 0.024 \pm 0.018.
\end{aligned}
\tag{1.1}$$

The SM predictions for $R(D)$ and $R(D^*)$ are [12, 13, 14]

$$\begin{aligned}
R(D) &= 0.297 \pm 0.017, \\
R(D^*) &= 0.252 \pm 0.003,
\end{aligned}
\tag{1.2}$$

which deviate from the BaBar measurements by 2σ and 2.7σ respectively. The BaBar collaboration reported a 3.4σ deviation from SM when the two measurements of Eq. (1.1) are taken together.

These deviations could be sign of NP and already certain models of NP have been considered to explain the data [13, 15, 16, 17, 18, 19, 20, 21, 22, 23, 24, 25, 26]. In Ref. [17], we calculated various observables in $\bar{B} \rightarrow D^+ \tau^- \bar{\nu}_\tau$ and $\bar{B} \rightarrow D^{*+} \tau^- \bar{\nu}_\tau$ decays with NP using an effective Lagrangian approach. The Lagrangian contains two quarks and two leptons with scalar, pseudoscalar, vector, axial vector and tensor operators. Considering the NP operators one at a time, the coefficient of these operators can be fixed from the BaBar measurements and then one can study the effect of these operators on the various observables. In this work, we extend the work of Ref. [17] by providing the full angular distribution for $\bar{B} \rightarrow D^{*+} \tau^- \bar{\nu}_\tau$ with NP. The full angular distribution, in the SM, has already been used in experiments for final states with muon and the electron. In this work we also consider CP violating observables which are the triple product (TP) asymmetries [27]. In the SM, these TPs rigorously vanish and so any non-zero measurements of these terms are clear signs of NP without any hadronic uncertainties. In the presence of NP with complex couplings the TP's are non-zero and depend on the form factors. Moreover, as we will see most of the TPs depend on the vector/axial vector couplings and not on the pseudoscalar couplings. Hence these TPs provide useful clues to the nature of NP. As in the previous work, we will neglect the tensor term in the effective Lagrangian.

The paper is organized in the following manner. In Sec. 2 we set up the formalism where we introduce the effective Lagrangian for NP, define the various helicity amplitudes and consider the constraints on the NP couplings. In Sec. 3 we present the angular distribution and define the various observables in $\bar{B} \rightarrow D^{*+} \tau^- \bar{\nu}_\tau$ decays. We present the SM predictions for these observables as well as predictions for the observables with NP. Finally, in Sec. 4 we summarize the results of our analysis.

2. Formalism

In the presence of NP, the effective Hamiltonian for the quark-level transition $b \rightarrow$

$cl^- \bar{\nu}_l$ can be written in the form [28]

$$\begin{aligned} \mathcal{H}_{eff} = \frac{4G_F V_{cb}}{\sqrt{2}} & \left[(1 + V_L) [\bar{c}\gamma_\mu P_L b] [\bar{l}\gamma^\mu P_L \nu_l] + V_R [\bar{c}\gamma^\mu P_R b] [\bar{l}\gamma_\mu P_L \nu_l] \right. \\ & \left. + S_L [\bar{c}P_L b] [\bar{l}P_L \nu_l] + S_R [\bar{c}P_R b] [\bar{l}P_L \nu_l] + T_L [\bar{c}\sigma^{\mu\nu} P_L b] [\bar{l}\sigma_{\mu\nu} P_L \nu_l] \right] \end{aligned} \quad (2.1)$$

where $G_F = 1.1663787(6) \times 10^{-5} GeV^{-2}$ is the Fermi coupling constant, V_{cb} is the Cabibbo-Kobayashi-Maskawa (CKM) matrix element, $P_{L,R} = (1 \mp \gamma_5)/2$ are the projectors of negative/positive chiralities. We use $\sigma_{\mu\nu} = i[\gamma_\mu, \gamma_\nu]/2$ and assume the neutrino to be always left chiral. Further, we do not assume any relation between $b \rightarrow ul^- \nu_l$ and $b \rightarrow cl^- \bar{\nu}_l$ transitions and hence do not include constraints from $B \rightarrow \tau \nu_\tau$. The SM effective Hamiltonian corresponds to $V_L = V_R = S_L = S_R = T_L = T_R = 0$. In this paper we will ignore the tensor interactions. With this simplification we write the effective Lagrangian as

$$\begin{aligned} \mathcal{H}_{eff} = \frac{G_F V_{cb}}{\sqrt{2}} & \left\{ \left[\bar{c}\gamma_\mu (1 - \gamma_5) b + g_V \bar{c}\gamma_\mu b + g_A \bar{c}\gamma_\mu \gamma_5 b \right] \bar{l}\gamma^\mu (1 - \gamma_5) \nu_l \right. \\ & \left. + \left[g_S \bar{c}b + g_P \bar{c}\gamma_5 b \right] \bar{l}(1 - \gamma_5) \nu_l + h.c. \right\}, \end{aligned} \quad (2.2)$$

where $g_{V,A} = V_R \pm V_L$ and $g_{S,P} = S_R \pm S_L$. The values of the couplings that can explain the data in Eq. (1.1) satisfy the constraints $|g_{V,A}| \lesssim 2$ and $|g_P| \lesssim 4$. One can consider if the size of these couplings can arise in typical extensions of the SM. Let us start with the vector/axial vector couplings and assume that the new physics is due to the exchange of a new particle with mass M_X with coupling g_{new} to the quarks which has the same size as the weak coupling, g , of the quarks to the W . One can then write

$$\frac{g_{new}^2}{8M_X^2} \approx \frac{g^2}{8M_W^2} V_{cb} g_{V,A}. \quad (2.3)$$

With $g_{new} \approx g$ one obtains,

$$g_{V,A} \approx \frac{M_W^2}{M_X^2 V_{cb}}. \quad (2.4)$$

Hence $M_X \approx 300$ GeV can lead to $g_{V,A} \approx 2$. Note that such a particle which couples dominantly to the third family is still allowed by experimental searches. Coming to the pseudoscalar coupling, one notes that the hadronic matrix elements are somewhat suppressed so larger values of g_P , satisfying $|g_P| \lesssim 4$, are needed to explain the data. In this case $M_X \approx 200$ GeV can lead to $g_P \approx 4$ and such a particle which couples dominantly to the third family is still allowed by experimental searches.

The effects of NP can be seen in the helicity amplitudes that describe the decays. The expressions for the hadronic helicity amplitudes for the $\bar{B} \rightarrow D^* \tau \bar{\nu}_\tau$ decays are

$$\begin{aligned}
\mathcal{A}_0 &= \frac{1}{2m_{D^*} \sqrt{q^2}} \left[(m_B^2 - m_{D^*}^2 - q^2)(m_B + m_{D^*})A_1(q^2) - \frac{4m_B^2 |p_{D^*}|^2}{m_B + m_{D^*}} A_2(q^2) \right] (1 - g_A), \\
\mathcal{A}_\parallel &= \sqrt{2}(m_B + m_{D^*})A_1(q^2)(1 - g_A), \\
\mathcal{A}_\perp &= -\sqrt{2} \frac{2m_B V(q^2)}{(m_B + m_{D^*})} |p_{D^*}| (1 + g_V), \\
\mathcal{A}_t &= \frac{2m_B |p_{D^*}| A_0(q^2)}{\sqrt{q^2}} (1 - g_A), \\
\mathcal{A}_P &= -\frac{2m_B |p_{D^*}| A_0(q^2)}{(m_b(\mu) + m_c(\mu))} g_P,
\end{aligned} \tag{2.5}$$

where the t and the P amplitudes arise in the combination

$$\mathcal{A}_{tP} = \left(\mathcal{A}_t + \frac{\sqrt{q^2}}{m_\tau} \mathcal{A}_P \right). \tag{2.6}$$

The form factors $A_{1,2,0}(q^2)$ and $V(q^2)$ are defined in the appendix. As is clear from the above equation, the various helicity amplitudes are sensitive to different NP operators. These helicity amplitudes can be probed in various differential distributions providing useful information about NP.

The transversity amplitudes \mathcal{A}_\parallel and \mathcal{A}_\perp are related to the helicity amplitudes \mathcal{A}_\pm as

$$\begin{aligned}
\mathcal{A}_\perp &= \frac{1}{\sqrt{2}} (\mathcal{A}_+ - \mathcal{A}_-), \\
\mathcal{A}_\parallel &= \frac{1}{\sqrt{2}} (\mathcal{A}_+ + \mathcal{A}_-).
\end{aligned} \tag{2.7}$$

All the amplitudes are complex if the NP couplings are complex. The phases in the couplings are weak phases and change sign when we go from particle to anti-particle decays. Though strong phases in the current can arise from higher-order loops these will be tiny and we will ignore them. Hence the only CP violating signals will be of the triple-product type and all direct CP violating effects will vanish. Moreover we see that $\mathcal{A}_{0,\parallel,t}$ have the same weak phases and any interference between these amplitudes will not lead to any CP violating signals. The only CP violating signals will come from the interference of \mathcal{A}_\perp with the other vector/axial vector and pseudoscalar current amplitudes $\mathcal{A}_{0,\parallel,tP}$.

We will now consider the two cases:

- Case a : In this case, we will set $S_L, S_R = 0$ and assume that the NP affects leptons of only the third generation. This scenario could arise from the exchange of a new charged W' boson [29]. We point out that this is just a simplifying

assumption and in fact the general angular distribution presented in the paper is also applicable to e and μ in the final state.

- Case b : In this case, we will set $V_L, V_R = 0$ and assume that the NP only affects leptons of the third generation. This scenario could arise in models with extended scalar sectors [30].

Finally, we discuss the possibility of long distance resonant contribution to this decay as one observes in $B \rightarrow K^{(*)}\ell^+\ell^-$ decays. Note that the decay $\bar{B} \rightarrow D^{*+}\tau^-\bar{\nu}_\tau$ is a tree level decay unlike $B \rightarrow K^{(*)}\ell^+\ell^-$. The decay can get long distance contributions from $B \rightarrow D^*X$ with the subsequent decay $X \rightarrow \tau\nu_\tau$ which is an annihilation process and is suppressed. The state X , given the energy required to produce the τ , can be $D_s^{(*)}, D^{(*)}$ e.t.c. The branching ratio for $B \rightarrow D^*X$ is smaller than $\bar{B} \rightarrow D^{*+}\tau^-\bar{\nu}_\tau$ and combined with the suppressed rate for $X \rightarrow \tau\nu_\tau$ the resonant long distance contribution in this case is much smaller than the leading tree level W exchange contribution and can be neglected.

2.1 Constraints on the NP couplings

For the numerical calculation, we use the $B \rightarrow D$ and $B \rightarrow D^*$ form factors in the heavy quark effective theory framework [31, 32]. $B \rightarrow D^*$ form factors are summarized in the appendix. The constraints on the complex NP couplings in the $b \rightarrow c\ell^-\bar{\nu}_\ell$ effective Hamiltonian come from the measured $R(D)$ and $R(D^*)$ in Eq. (1.1) at 95% C.L. We also vary the free parameters in the form factors discussed in the appendix within their error bars. All the other numerical values are taken from [33] and [34]. A detailed analysis of $R(D)$ and NP in the decay $\bar{B} \rightarrow D^+\ell^-\bar{\nu}_\ell$ can be found in [17]. The allowed ranges for the NP couplings are then used for predicting the allowed ranges for the observables in the the angular distribution discussed in the next section. The experimental results show a correlation between $R(D)$ and $R(D^*)$. Many NP models would affect both $R(D)$ and $R(D^*)$ and produce a correlation between them, while other NP models would affect only one of the ratios. We believe the measured deviations from the SM for both $R(D)$ and $R(D^*)$ are not significant enough to rule out the SM or NP models that affect only one of the ratios. Hence, in our determination of the allowed ranges of the NP couplings the correlations between $R(D)$ and $R(D^*)$ are not taken into account. In the future, if experiments find more significant deviations from the SM predictions for the two ratios, or other clear signals for NP in these decays, then the effect of the correlation will have to be taken into account to find the nature of the NP. The goal of the paper is to point out how different observables in these decays can to be used to find NP and the nature of the NP.

The combination of the couplings $g_V = V_R + V_L$ appears in both $R(D)$ and $R(D^*)$, while $g_A = V_R - V_L$ appears only in $R(D^*)$. V_R and V_L receive constraints from both

$R(D)$ and $R(D^*)$. If NP is established in both $R(D)$ and $R(D^*)$ then the case of pure g_A coupling is ruled out. The constraints on the complex couplings g_V and g_A are shown in the colored region of Fig. 1 (left) and (right). We confirm from Eq. (2.5) that if the new interaction is purely left-handed then the amplitudes and all the distributions just get scaled by a common factor. Hence, instead of considering the pure $V - A$ and $V + A$ quark current cases, we will consider cases which include pure g_V or pure g_A complex couplings. Interestingly, the analysis in Ref. [17] indicates that the data prefers either pure vector or pure axial vector couplings.

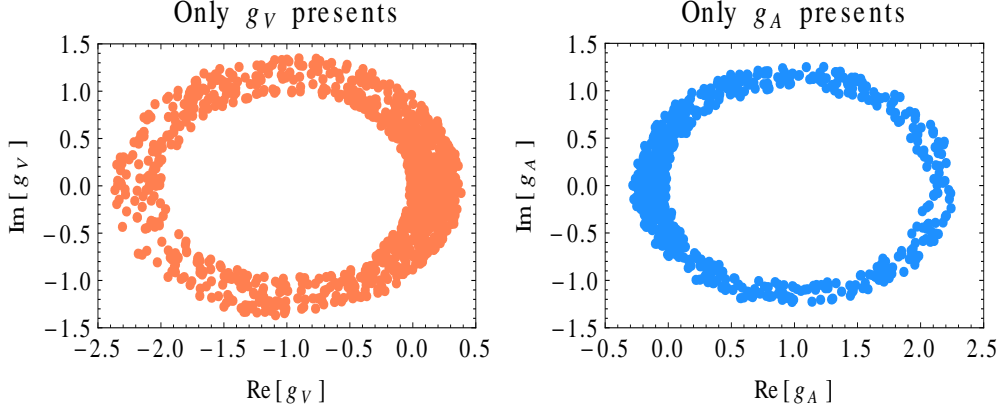


Figure 1: The constraints on the complex coupling $g_V = V_R + V_L$ (left panel) and on the complex couplings $g_A = V_R - V_L$ (right panel) at 95% C.L.

The combination of the couplings $g_S = S_R + S_L$ appears only in $R(D)$, while $g_P = S_R - S_L$ appears only in $R(D^*)$. If NP is established in both $R(D)$ and $R(D^*)$ then the cases of pure g_S or g_P couplings will be ruled out. The constraints on the complex couplings g_S and g_P are shown in Fig. 2.

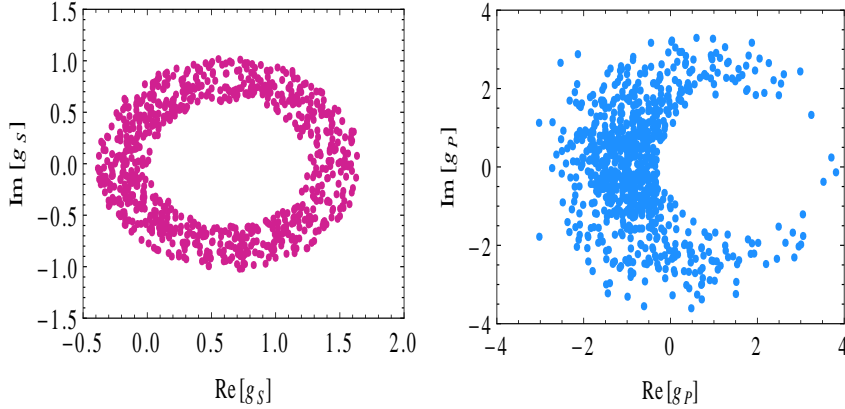


Figure 2: The constraints on the complex coupling g_S (left panel) and on the complex coupling g_P (right panel) at 95% C.L. .

3. Angular analysis

The complete three-angle distribution for the decay $\bar{B} \rightarrow D^*(\rightarrow D\pi)l^-\bar{\nu}_l$ in the presence of NP can be expressed in terms of four kinematic variables q^2 , two polar angles θ_l, θ_{D^*} , and the azimuthal angle χ . The angle θ_l is the polar angle between the charged lepton and the direction opposite to the D^* meson in the $(l\nu_l)$ rest frame. The angle θ_{D^*} is the polar angle between the D meson and the direction of the D^* meson in the $(D\pi)$ rest frame. The angle χ is the azimuthal angle between the two decay planes spanned by the 3-momenta of the $(D\pi)$ and $(l\nu_l)$ systems. These angles are described in Fig. 3. The three-angle distribution can be obtained by using the helicity formalism.

We can write the angular distribution explicitly for easy comparison with previous literature [35, 36, 37, 38]

$$\frac{d^4\Gamma}{dq^2 d\cos\theta_l d\cos\theta_{D^*} d\chi} = \frac{9}{32\pi} N_F \left(\sum_{i=1}^8 I_i + \frac{m_l^2}{q^2} \sum_{j=1}^8 J_j \right), \quad (3.1)$$

where

$$\begin{aligned} I_1 &= 4 \cos^2 \theta_{D^*} \sin^2 \theta_l |\mathcal{A}_0|^2, \\ J_1 &= 4 \cos^2 \theta_{D^*} \left[|\mathcal{A}_0|^2 \cos^2 \theta_l + |\mathcal{A}_{tP}|^2 - 2 \text{Re}[\mathcal{A}_{tP} \mathcal{A}_0^*] \cos \theta_l \right], \\ I_2 &= \sin^2 \theta_{D^*} \left[(|\mathcal{A}_{\parallel}|^2 + |\mathcal{A}_{\perp}|^2)(1 + \cos^2 \theta_l) - 4 \text{Re}[\mathcal{A}_{\parallel} \mathcal{A}_{\perp}^*] \cos \theta_l \right], \\ J_2 &= \sin^2 \theta_{D^*} \sin^2 \theta_l (|\mathcal{A}_{\parallel}|^2 + |\mathcal{A}_{\perp}|^2), \\ I_3 &= -\sin^2 \theta_{D^*} \sin^2 \theta_l \cos 2\chi (|\mathcal{A}_{\parallel}|^2 - |\mathcal{A}_{\perp}|^2), \\ J_3 &= \sin^2 \theta_{D^*} \sin^2 \theta_l \cos 2\chi (|\mathcal{A}_{\parallel}|^2 - |\mathcal{A}_{\perp}|^2), \\ I_4 &= -2\sqrt{2} \sin 2\theta_{D^*} \sin \theta_l \cos \chi \text{Re}[\mathcal{A}_{\perp} \mathcal{A}_0^*], \\ J_4 &= 2\sqrt{2} \sin 2\theta_{D^*} \sin \theta_l \cos \chi \text{Re}[\mathcal{A}_{\parallel} \mathcal{A}_{tP}^*], \\ I_5 &= 2\sqrt{2} \sin 2\theta_{D^*} \sin \theta_l \cos \theta_l \cos \chi \text{Re}[\mathcal{A}_{\parallel} \mathcal{A}_0^*], \\ J_5 &= -2\sqrt{2} \sin 2\theta_{D^*} \sin \theta_l \cos \theta_l \cos \chi \text{Re}[\mathcal{A}_{\parallel} \mathcal{A}_0^*], \\ I_6 &= \sin^2 \theta_{D^*} \sin^2 \theta_l \sin 2\chi \text{Im}[\mathcal{A}_{\parallel} \mathcal{A}_{\perp}^*], \\ J_6 &= -\sin^2 \theta_{D^*} \sin^2 \theta_l \sin 2\chi \text{Im}[\mathcal{A}_{\parallel} \mathcal{A}_{\perp}^*], \\ I_7 &= -2\sqrt{2} \sin 2\theta_{D^*} \sin \theta_l \sin \chi \text{Im}[\mathcal{A}_{\parallel} \mathcal{A}_0^*], \\ J_7 &= -2\sqrt{2} \sin 2\theta_{D^*} \sin \theta_l \sin \chi \text{Im}[\mathcal{A}_{\perp} \mathcal{A}_{tP}^*], \\ I_8 &= \sqrt{2} \sin 2\theta_{D^*} \sin 2\theta_l \sin \chi \text{Im}[\mathcal{A}_{\perp} \mathcal{A}_0^*], \\ J_8 &= -\sqrt{2} \sin 2\theta_{D^*} \sin 2\theta_l \sin \chi \text{Im}[\mathcal{A}_{\perp} \mathcal{A}_0^*], \end{aligned} \quad (3.2)$$

where the quantity N_F is

$$N_F = \left[\frac{G_F^2 |p_{D^*}| |V_{cb}|^2 q^2}{3 \times 2^6 \pi^3 m_B^2} \left(1 - \frac{m_l^2}{q^2} \right)^2 \text{Br}(D^* \rightarrow D\pi) \right]. \quad (3.3)$$

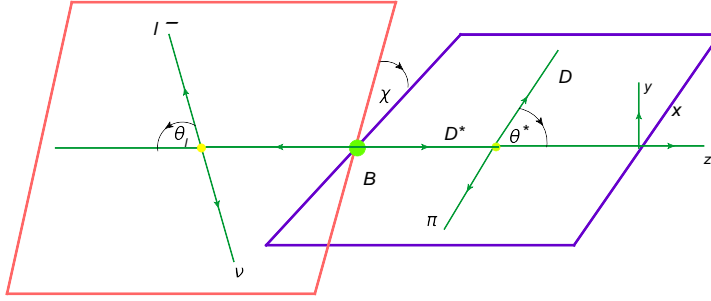


Figure 3: The description of the angles θ_{l,D^*} and χ in the angular distribution of $\bar{B} \rightarrow D^*(\rightarrow D\pi)l^-\nu_l$ decay.

The momentum of the D^* meson in the B meson rest frame is denoted as $|p_{D^*}| = \lambda^{1/2}(m_B^2, m_{D^*}^2, q^2)/2m_B$ with $\lambda(a, b, c) = a^2 + b^2 + c^2 - 2(ab + bc + ca)$. When there are no strong phases then \mathcal{A}_{\parallel} and \mathcal{A}_0 have the same weak phase and I_7 vanishes.

The complex NP couplings lead to CP violation which are sensitive to the angular terms $\sin \chi$ and $\sin 2\chi$. The coefficients of these terms are TPs and have the structure $\sim \text{Im}[\mathcal{A}_i \mathcal{A}_j^*] \sim \sin(\phi_i - \phi_j)$, where $\mathcal{A}_{i,j} = |\mathcal{A}_{i,j}| e^{i\phi_{i,j}}$. In the SM these terms vanish, to a very good approximation, as there is only one dominant contribution to the decay and so all amplitudes have the same weak phase. Hence any non-zero measurements of the TPs are clear signs of NP without any hadronic uncertainties. For the charged conjugate modes, the weak phases change sign and $\bar{\mathcal{A}}_{i,j} = |\mathcal{A}_{i,j}| e^{-i\phi_{i,j}}$ and the TPs change sign. Even though we focus on τ final states, we should point out that this distribution is applicable also for e and μ in the final state. Since experiments have already studied this distribution for e, μ final states it might be worth checking the $\sin \chi$ and $\sin 2\chi$ terms in the distributions for these decays for signals of non-SM physics.

It will be convenient to rewrite the angular distribution as [39],

$$\begin{aligned} \frac{d^4\Gamma}{dq^2 d\cos\theta_l d\cos\theta_{D^*} d\chi} = \frac{9}{32\pi} NF \left\{ \begin{aligned} &\cos^2\theta_{D^*} \left(V_1^0 + V_2^0 \cos 2\theta_l + V_3^0 \cos \theta_l \right) \\ &+ \sin^2\theta_{D^*} \left(V_1^T + V_2^T \cos 2\theta_l + V_3^T \cos \theta_l \right) \\ &+ V_4^T \sin^2\theta_{D^*} \sin^2\theta_l \cos 2\chi + V_1^{0T} \sin 2\theta_{D^*} \sin 2\theta_l \cos \chi \\ &+ V_2^{0T} \sin 2\theta_{D^*} \sin \theta_l \cos \chi + V_5^T \sin^2\theta_{D^*} \sin^2\theta_l \sin 2\chi \\ &+ V_3^{0T} \sin 2\theta_{D^*} \sin \theta_l \sin \chi + V_4^{0T} \sin 2\theta_{D^*} \sin 2\theta_l \sin \chi \end{aligned} \right\}. \end{aligned} \quad (3.4)$$

The decay $\bar{B} \rightarrow D^*(\rightarrow D\pi)l^-\bar{\nu}_l$ is completely described in terms of twelve angular coefficient functions V_i . These angular coefficients depend on the couplings, kinematic

variables and form factors, and are given in the Appendix in Eq. (B.7), Eq. (B.8) and Eq. (B.9).

For the CP-conjugate decay $B \rightarrow \bar{D}^*(\rightarrow D\pi)l^+\nu_l$, one defines the angles relative to the directions of the τ^+ and \bar{D}^* . The \bar{V}_i 's can be obtained from the V_i 's by replacing $\theta_l \rightarrow \theta_l + \pi$ and $\chi \rightarrow -\chi$, and changing the signs of the weak phases. This transformation is equivalent to replacing $V_{1,2}^0 \rightarrow \bar{V}_{1,2}^0$, $V_3^0 \rightarrow -\bar{V}_3^0$, $V_{1,2,4}^T \rightarrow \bar{V}_{1,2,4}^T$, $V_{3,5}^T \rightarrow -\bar{V}_{3,5}^T$, $V_{1,3}^{0T} \rightarrow \bar{V}_{1,3}^{0T}$, and $V_{2,4}^{0T} \rightarrow -\bar{V}_{2,4}^{0T}$. The angular distribution for the CP-conjugate process is

$$\begin{aligned} \frac{d^4\bar{\Gamma}}{dq^2 d\cos\theta_l d\cos\theta_{D^*} d\chi} = \frac{9}{32\pi} N_F \left\{ \begin{aligned} & \cos^2\theta_{D^*} \left(\bar{V}_1^0 + \bar{V}_2^0 \cos 2\theta_l - \bar{V}_3^0 \cos\theta_l \right) \\ & + \sin^2\theta_{D^*} \left(\bar{V}_1^T + \bar{V}_2^T \cos 2\theta_l - \bar{V}_3^T \cos\theta_l \right) \\ & + \bar{V}_4^T \sin^2\theta_{D^*} \sin^2\theta_l \cos 2\chi + \bar{V}_1^{0T} \sin 2\theta_{D^*} \sin 2\theta_l \cos\chi \\ & - \bar{V}_2^{0T} \sin 2\theta_{D^*} \sin\theta_l \cos\chi - \bar{V}_5^T \sin^2\theta_{D^*} \sin^2\theta_l \sin 2\chi \\ & + \bar{V}_3^{0T} \sin 2\theta_{D^*} \sin\theta_l \sin\chi - \bar{V}_4^{0T} \sin 2\theta_{D^*} \sin 2\theta_l \sin\chi \end{aligned} \right\}. \end{aligned} \quad (3.5)$$

3.1 Differential branching ratio

The angular distribution allows us to define several observables. The starting point is to obtain the differential distribution $d\Gamma/dq^2$ after performing integration over all the angles

$$\frac{d\Gamma}{dq^2} = \frac{3N_F}{4} (A_L + A_T), \quad (3.6)$$

where the D^* longitudinal and transverse polarization amplitudes A_L and A_T are

$$A_L = \left(V_1^0 - \frac{1}{3}V_2^0 \right), \quad A_T = 2 \left(V_1^T - \frac{1}{3}V_2^T \right). \quad (3.7)$$

One can see from Eq. (B.7) and Eq. (B.8) that A_L is proportional to $|\mathcal{A}_0|^2$ and $|\mathcal{A}_{tP}|^2$ while A_T to $|\mathcal{A}_\parallel|^2 + |\mathcal{A}_\perp|^2$. The D^* polarization amplitudes can be extracted from the angular distribution in $\cos\theta_{D^*}$ (see Eq. (3.10) below). Since there is no direct CP violation, we have $A_{L,T} = \bar{A}_{L,T}$. Hence,

$$\frac{d\Gamma}{dq^2} = \frac{d\bar{\Gamma}}{dq^2}. \quad (3.8)$$

Furthermore, one can also explore the q^2 dependent ratio

$$R_{D^*}(q^2) = \frac{dBr[\bar{B} \rightarrow D^{*+}\tau^-\bar{\nu}_\tau]/dq^2}{dBr[\bar{B} \rightarrow D^*\ell^-\bar{\nu}_\ell]/dq^2}, \quad (3.9)$$

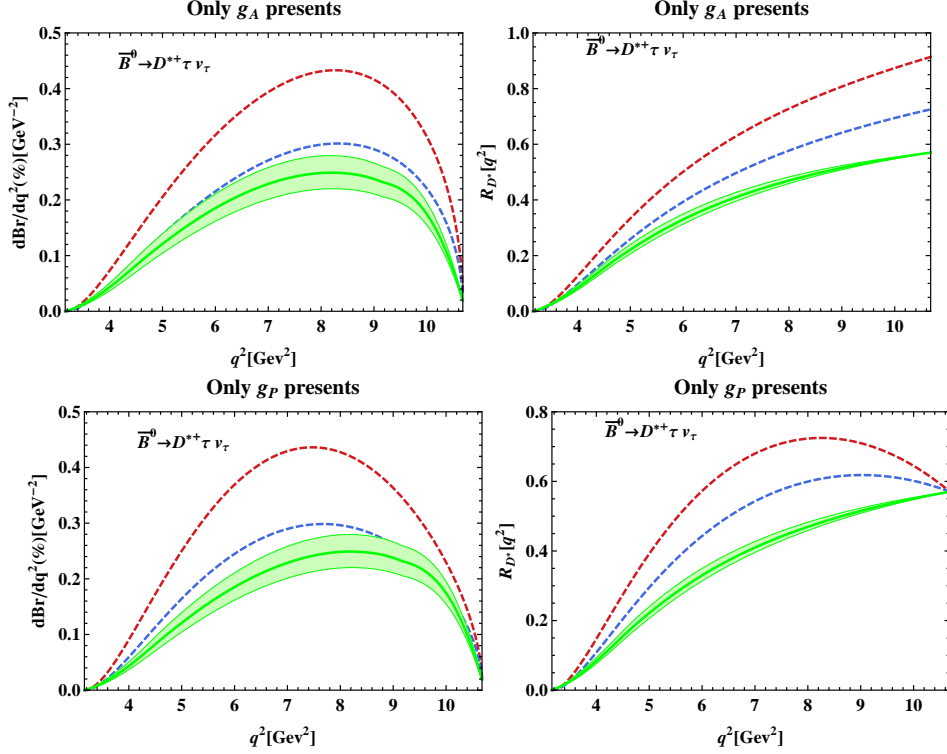


Figure 4: The left (right) panels of the figure show the differential branching ratio ($R_{D^*}(q^2)$) for the decay $\bar{B}^0 \rightarrow D^{*+} \tau \nu_\tau$ in the scenario where only g_A (upper) and only g_P (lower) couplings are present. The green band corresponds to the SM prediction and its uncertainties. The red and blue dashed lines correspond to $|g_A|e^{i\phi_{g_A}} = 0.62e^{i1.74}$ and $|g_A|e^{i\phi_{g_A}} = 0.13e^{i2.63}$ respectively, in the upper-left panel, and $|g_A|e^{i\phi_{g_A}} = 0.34e^{i2.38}$ and $|g_A|e^{i\phi_{g_A}} = 0.73e^{i1.39}$ in the upper-right panel. The red and blue dashed lines correspond to $|g_P|e^{i\phi_{g_P}} = 2.27e^{-i2.92}$ and $|g_P|e^{i\phi_{g_P}} = 1.65e^{-i2.96}$ in the lower-left panel, and $|g_P|e^{i\phi_{g_P}} = 2.56e^{-i2.17}$ and $|g_P|e^{i\phi_{g_P}} = 2.60e^{-i1.95}$ in the lower-right panel. The values of the couplings are chosen to show the maximum and minimum deviations from the SM expectations.

where l denotes the light lepton (e, μ). The ratio R_{D^*} are independent of the form factor $h_{A_1}(w)$.

Fig. 4 shows the differential branching ratio (DBR) and $R_{D^*}(q^2)$ for $\bar{B}^0 \rightarrow D^{*+} \tau \nu_\tau$ in the presence of only $g_A = V_R - V_L$ and only $g_P = S_R - S_L$ couplings. We make the following observations:

- If only the g_A coupling is present, the DBR can be enhanced up to 0.4% at $q^2 \approx 8.5 \text{ GeV}^2$. $R_{D^*}(q^2)$ can be enhanced up to 0.9% at high q^2 . The shape of the distribution is similar to that in the SM.
- If only the g_P coupling is present, the DBR can be enhanced up to 0.4% at $q^2 \approx 7.5 \text{ GeV}^2$. Note that the peak of the DBR is shifted to the low q^2 direction

relative to the SM. $R_{D^*}(q^2)$ is approximately 0.7 at $q^2 \approx 7.5\text{GeV}^2$. The shape of the distribution is different from that in the SM.

Finally, the new NP coupling g_V only appears in the transverse amplitude \mathcal{A}_\perp , and does not significantly affect the DBR and $R_{D^*}(q^2)$. The shape of the distribution is again similar to that in the SM.

We note that recently BaBar has reported the measurement of the differential distribution for both $\bar{B} \rightarrow D^{*+}\tau^-\bar{\nu}_\tau$ and $\bar{B} \rightarrow D^+\tau^-\bar{\nu}_\tau$ decays [40] and the results seem to generally favor vector, axial-vector type NP though scalar/pseudoscalar NP are not ruled out.

3.2 Polarization fraction for D^*

The differential angular distribution in $\cos\theta_{D^*}$ gives access to the polarization fraction of the D^* meson in the decay $\bar{B} \rightarrow D^*(\rightarrow D\pi)\tau^-\bar{\nu}_\tau$

$$\frac{d^2\Gamma}{dq^2 d\cos\theta_{D^*}} = \frac{1}{4} \frac{d\Gamma}{dq^2} (2F_L^{D^*} \cos^2\theta_{D^*} + (1 - F_L^{D^*}) \sin^2\theta_{D^*}), \quad (3.10)$$

where we define the longitudinal and transverse polarization fractions of the D^* meson as

$$F_L^{D^*}(q^2) = \frac{A_L}{A_L + A_T}, \quad F_T^{D^*}(q^2) = \frac{A_T}{A_L + A_T}, \quad (3.11)$$

with $F_L^{D^*}(q^2) + F_T^{D^*}(q^2) = 1$. Similarly, one can define the polarization fractions $\bar{F}_{L,T}^{D^*}(q^2)$ for the CP-conjugate mode but they are the same as $F_{L,T}^{D^*}(q^2)$ in the absence of direct CP violation.

When only the coupling g_A is present, the polarization fractions of the D^* meson gets contributions from the amplitudes \mathcal{A}_0 and \mathcal{A}_\parallel , which are functions of the new g_A coupling. Due to cancellation of the g_A coupling contributions in $F_L^{D^*}(q^2)$, its behavior is similar to its SM prediction. New g_V coupling appears only in the amplitude A_\perp and again $F_L^{D^*}(q^2)$ looks similar to its SM prediction. In Fig. 5, we show $F_L^{D^*}(q^2)$ and the ratio $r_{F_L} = [F_L^{D^*}]^{NP+SM}/[F_L^{D^*}]^{SM} - 1 = [F_L^{D^*}]^{NP}/[F_L^{D^*}]^{SM}$ in the presence of the g_P coupling. In this case $F_L^{D^*}(q^2)$ can be as large as 0.85 at low q^2 , and it decreases to the SM value at high q^2 while the ratio r_{F_L} reaches 40% around $q^2 \approx 8.0 \text{ GeV}^2$.

The q^2 -integrated polarization fractions $\langle F_{L,T}^{D^*} \rangle$ can be obtained by separately integrating out the numerator and the denominator in Eq. (3.11). We obtain $\langle F_L^{D^*} \rangle_{SM} \approx 0.53$ in the SM for the $\bar{B}^0 \rightarrow D^{*+}\tau\nu_\tau$ decay and only the new g_P coupling can enhance $\langle F_L^{D^*} \rangle$ by about 6% from its SM value.

3.3 Distribution in $\cos\theta_l$ and A_{FB}

The forward-backward asymmetry A_{FB} can be obtained from the single-differential angular distribution

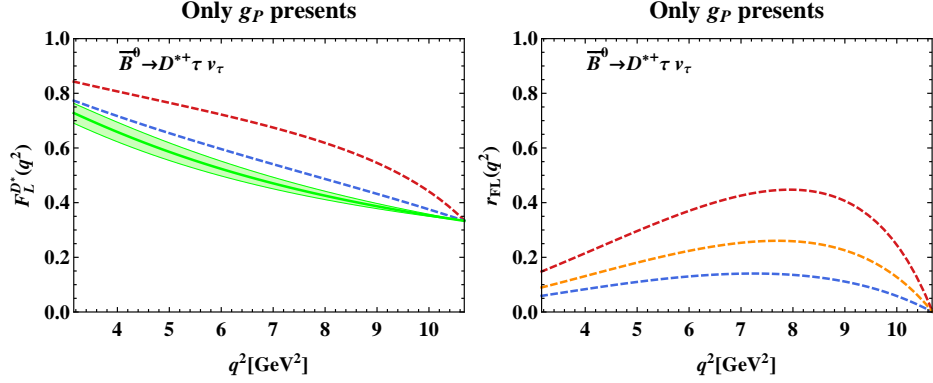


Figure 5: The left and right panels of the figure show $F_L^{D^*}$ and the ratio r_{FL} for the decay $\bar{B} \rightarrow D^{*+} \tau^- \bar{\nu}_\tau$ in the scenario where only the g_P coupling is present. The green band corresponds to the SM prediction and its uncertainties. The red and blue dashed lines correspond to $|g_P|e^{i\phi_{gP}} = 2.27e^{-i2.92}$ and $|g_P|e^{i\phi_{gP}} = 0.90e^{-i2.74}$ respectively. The values of the couplings are chosen to show the maximum and minimum deviations from the SM expectations.

$$\frac{d^2\Gamma}{dq^2 d\cos\theta_l} = \frac{3N_F}{4} \left[\left(V_1^T + \frac{1}{2}V_1^0 \right) + \left(V_2^T + \frac{1}{2}V_2^0 \right) \cos 2\theta_l + \left(V_3^T + \frac{1}{2}V_3^0 \right) \cos \theta_l \right], \quad (3.12)$$

The forward-backward asymmetry (FBA) for the leptons is defined by

$$A_{FB}(q^2) = \frac{\int_0^1 d\cos\theta_l \frac{d^2\Gamma}{dq^2 d\cos\theta_l} - \int_{-1}^0 d\cos\theta_l \frac{d^2\Gamma}{dq^2 d\cos\theta_l}}{\int_0^1 d\cos\theta_l \frac{d^2\Gamma}{dq^2 d\cos\theta_l} + \int_{-1}^0 d\cos\theta_l \frac{d^2\Gamma}{dq^2 d\cos\theta_l}}. \quad (3.13)$$

Then one can obtain:

$$A_{FB}(q^2) = \frac{V_3^T + \frac{1}{2}V_3^0}{A_L + A_T}, \quad (3.14)$$

similarly, FBA for the conjugate mode is

$$\bar{A}_{FB}(q^2) = - \left[\frac{\bar{V}_3^T + \frac{1}{2}\bar{V}_3^0}{\bar{A}_L + \bar{A}_T} \right]. \quad (3.15)$$

If the absence of direct CP violation, $\bar{A}_{FB}(q^2) = -A_{FB}(q^2)$. We define the average FBA as

$$A_{FB}^{D^*}(q^2) = \frac{1}{2} \left(A_{FB}(q^2) - \bar{A}_{FB}(q^2) \right). \quad (3.16)$$

Within the SM, $A_{FB}^{D^*}(q^2)$ has a zero crossing at $q^2 \approx 5.64\text{GeV}^2$ (see Fig. (6)). We make the following observations from this figure

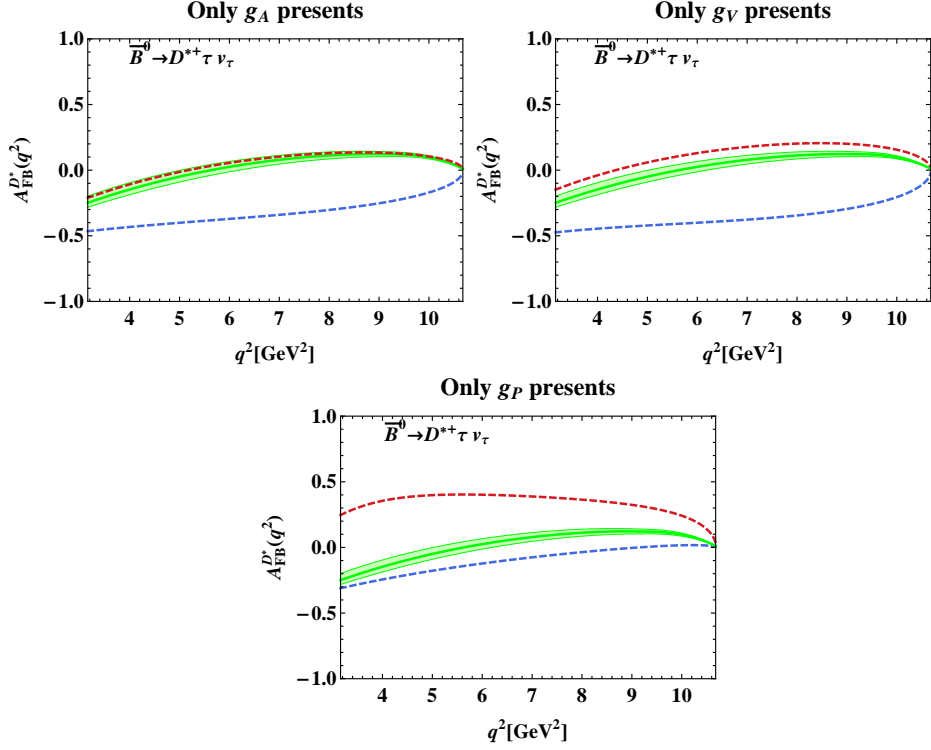


Figure 6: The figures show $A_{FB}^{D^*}(q^2)$ for the decay $\bar{B}^0 \rightarrow D^{*+} \tau^- \bar{\nu}_\tau$ in the scenario where only g_A , g_V and g_P couplings are present. The green band corresponds to the SM prediction and its uncertainties. The red and blue dashed lines correspond to $|g_A|e^{i\phi_{g_A}} = 0.1e^{i2.19}$ and $|g_A|e^{i\phi_{g_A}} = 2.06e^{i0.1}$ respectively, in the upper-left panel, $|g_V|e^{i\phi_{g_V}} = 0.48e^{-i0.84}$ and $|g_V|e^{i\phi_{g_V}} = 2.23e^{i2.94}$ in the upper-right panel, and $|g_P|e^{i\phi_{g_P}} = 3.53e^{-i0.11}$ and $|g_P|e^{i\phi_{g_P}} = 1.69e^{-i2.94}$ in the lower panel. The values of the couplings are chosen to show the maximum and minimum deviations from the SM expectations.

- If only the g_A or only the g_V couplings are present, the FBA can reach a value close to 50% at low q^2 and its sign is mostly negative. The FBA converges to its SM prediction at high q^2 .
- If only the g_P coupling is present, the FBA can reach a value up to 30% at low q^2 . It can have both positive or negative signs. Again, the FBA converges to its SM prediction at high q^2 .

In Table.1 we summarize the predictions for the q^2 -integrated FBA $\langle A_{FB}^{D^*} \rangle$ for the decay $\bar{B}^0 \rightarrow D^{*+} \tau \nu_\tau$.

3.4 Asymmetries $A_C^{(i)}$ in the angular variable χ

In this section, we consider three different transverse asymmetries $A_C^{(i=1,2,3)}$. These asymmetries are obtained by integrating out the polar angles θ_l and θ_{D^*} in three different regions.

Table 1: Predictions for the q^2 -integrated FBA $\langle A_{FB}^{D^*} \rangle$ both within the SM and in the presence of different NP couplings for the decay $\bar{B}^0 \rightarrow D^{*+} \tau \nu_\tau$.

	SM Prediction	Only g_A	Only g_V	Only g_P
$\langle A_{FB}^{D^*} \rangle$	-0.041	[-0.055, -0.349]	[-0.382, 0.045]	[-0.127, 0.343]

3.4.1 $A_C^{(1)}$

The transverse asymmetry $A_C^{(1)}$ is defined through the angular distribution in χ as

$$\frac{d^2\Gamma}{dq^2 d\chi} = \frac{1}{2\pi} \frac{d\Gamma}{dq^2} \left[1 + \left(A_C^{(1)} \cos 2\chi + A_T^{(1)} \sin 2\chi \right) \right]. \quad (3.17)$$

It can be obtained by integrating Eq. (3.4) over the two polar angles θ_l and θ_{D^*} . Here $A_T^{(1)}$ is a TP, and is discussed separately below. One can obtain

$$A_C^{(1)}(q^2) = \frac{4V_4^T}{3(A_L + A_T)}, \quad (3.18)$$

and similarly, for the conjugate mode

$$\bar{A}_C^{(1)}(q^2) = \frac{4\bar{V}_4^T}{3(\bar{A}_L + \bar{A}_T)}. \quad (3.19)$$

In the absence of direct CP violation $\bar{A}_C^{(1)} = A_C^{(1)}$. We define the average $A_C^{(1)}(q^2)$ as

$$\langle A_C^{(1)}(q^2) \rangle = \frac{1}{2} \left(A_C^{(1)}(q^2) + \bar{A}_C^{(1)}(q^2) \right). \quad (3.20)$$

The SM prediction for $\langle A_C^{(1)}(q^2) \rangle$ is shown in the green band of Fig. 7(left panel). Similar to $F_L^{D^*}$, the asymmetry $\langle A_C^{(1)}(q^2) \rangle$ remains almost the same as the SM prediction when only the g_A or only the g_V couplings are presents.

The g_P coupling appears only in the amplitude A_P and affects only the denominator of $A_C^{(1)}(q^2)$. The amplitude A_P vanishes at high q^2 , and hence $\langle A_C^{(1)}(q^2) \rangle$ reduces to its SM value as shown in Fig. 7(left panel). The magnitude of the ratio $r_1(q^2) = [A_C^{(1)}(q^2)]^{SM+NP} / [A_C^{(1)}(q^2)]^{SM} - 1 = [A_C^{(1)}(q^2)]^{NP} / [A_C^{(1)}(q^2)]^{SM}$ reaches more than 25% at $q^2 \approx 5.0 \text{ GeV}^2$ as shown in Fig. 7(right panel).

3.4.2 $A_C^{(2)}$

We define the angular distribution

$$\frac{d^2\Gamma^{(2)}}{dq^2 d\chi} = \left[\int_0^1 - \int_{-1}^0 \right] \frac{d^4\Gamma}{dq^2 d\cos\theta_l d\cos\theta_{D^*} d\chi} d\cos\theta_{D^*}. \quad (3.21)$$

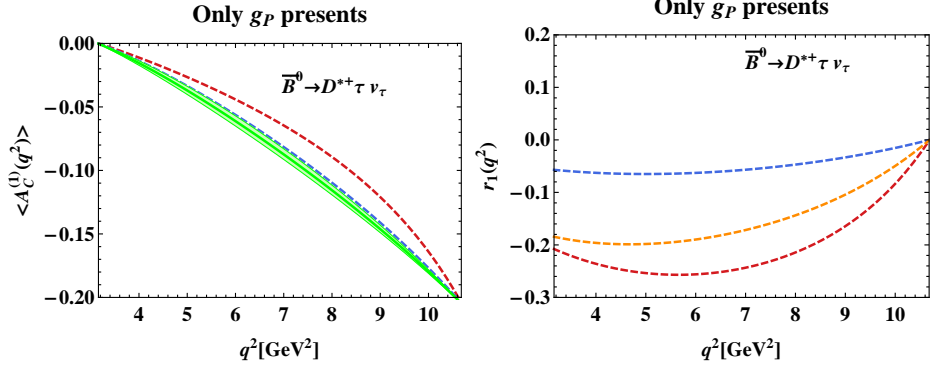


Figure 7: The figure shows $\langle A_C^{(1)}(q^2) \rangle$ and $r_1(q^2)$ for the decay $\bar{B} \rightarrow D^{*+} \tau^- \bar{\nu}_\tau$ in the scenario where only the g_P coupling is present. The green band corresponds to the SM prediction and its uncertainties. The red and blue dashed lines correspond to $|g_P|e^{i\phi_{gP}} = 2.17e^{i1.75}$ and $|g_P|e^{i\phi_{gP}} = 0.68e^{-i1.79}$ respectively. The values of the couplings are chosen to show the maximum and minimum deviations from the SM expectations.

One can obtain

$$\frac{d^2\Gamma^{(2)}}{dq^2 d\chi} = \frac{1}{4} \frac{d\Gamma}{dq^2} \left[A_C^{(2)} \cos \chi + A_T^{(2)} \sin \chi \right], \quad (3.22)$$

where

$$A_C^{(2)}(q^2) = \frac{V_2^{0T}}{(A_L + A_T)}. \quad (3.23)$$

Here $A_T^{(2)}$ is a TP, and is discussed separately below. For the conjugate mode

$$\bar{A}_C^{(2)}(q^2) = \frac{-\bar{V}_2^{0T}}{(\bar{A}_L + \bar{A}_T)}. \quad (3.24)$$

In the absence of direct CP violation $\bar{A}_C^{(2)} = -A_C^{(2)}$. We define the average $A_C^{(2)}(q^2)$ as

$$\langle A_C^{(2)}(q^2) \rangle = \frac{1}{2} \left(A_C^{(2)}(q^2) - \bar{A}_C^{(2)}(q^2) \right). \quad (3.25)$$

$\langle A_C^{(2)}(q^2) \rangle$ depends on all the three couplings g_A , g_V , and g_P . For all q^2 , the magnitude of $\langle A_C^{(2)}(q^2) \rangle$ is generally suppressed by these new couplings. As shown in Fig. 8, in all three cases, the value of $\langle A_C^{(2)}(q^2) \rangle$ can be either positive or negative. In particular, there may or may not be a non-SM zero crossing.

The q^2 dependence of the ratio $r_2(q^2) = [A_C^{(2)}(q^2)]^{SM+NP} / [A_C^{(2)}(q^2)]^{SM} - 1 = [A_C^{(2)}(q^2)]^{NP} / [A_C^{(2)}(q^2)]^{SM}$ is shown in Fig. 9 for all the three cases. The magnitude of $r_2(q^2)$ can be more than 100% at high q^2 .

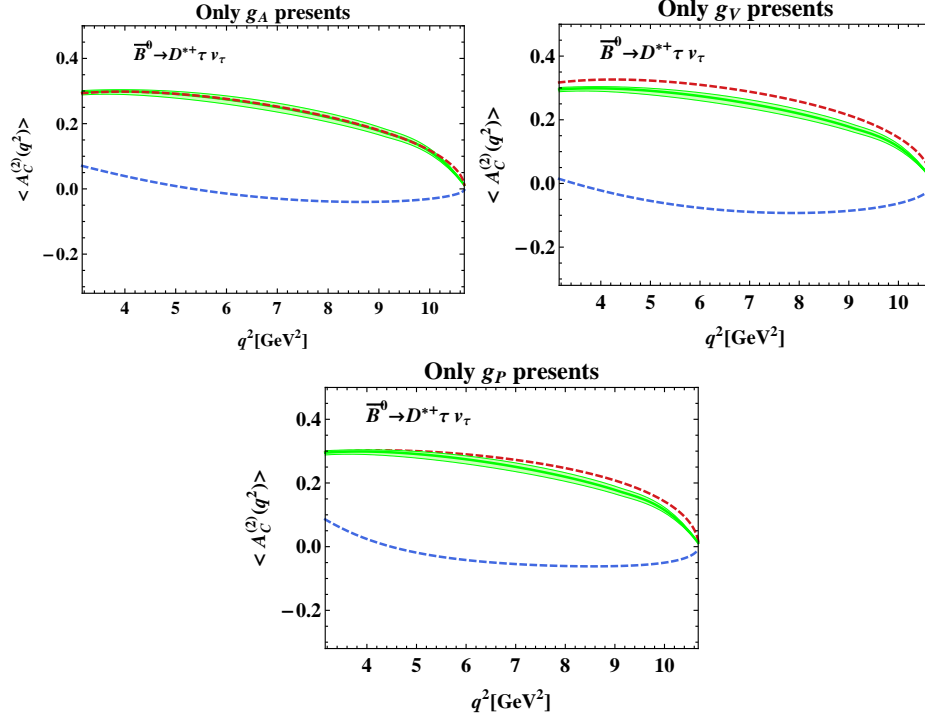


Figure 8: The figures show $\langle A_C^{(2)}(q^2) \rangle$ for the decay $\bar{B}^0 \rightarrow D^{*+} \tau \nu_\tau$ in the scenario where only g_A , only g_V and only g_P couplings are present. The green band corresponds to the SM prediction and its uncertainties. The red and blue dashed lines correspond to $|g_A|e^{i\phi_{g_A}} = 0.04e^{i2.83}$ and $|g_A|e^{i\phi_{g_A}} = 2.06e^{i0.1}$ respectively, in the upper-left panel, $|g_V|e^{i\phi_{g_V}} = 0.34e^{i0.28}$ and $|g_V|e^{i\phi_{g_V}} = 2.37e^{-i3.12}$ in the upper-right panel, and $|g_P|e^{i\phi_{g_P}} = 0.82e^{-i2.67}$ and $|g_P|e^{i\phi_{g_P}} = 3.80e^{-i0.04}$ in the lower panel. The values of the couplings are chosen to show the maximum and minimum deviations from the SM expectations.

3.4.3 $A_C^{(3)}$

Finally, we define the single angle distribution

$$\frac{d^2\Gamma^{(3)}}{dq^2 d\chi} = \left[\int_0^1 - \int_{-1}^0 \right] d\cos\theta_l \left[\int_0^1 - \int_{-1}^0 \right] d\cos\theta_{D^*} \frac{d^4\Gamma}{dq^2 d\cos\theta_l d\cos\theta_{D^*} d\chi}. \quad (3.26)$$

One can obtain

$$\frac{d^2\Gamma^{(3)}}{dq^2 d\chi} = \frac{2}{3\pi} \frac{d\Gamma}{dq^2} \left[A_C^{(3)} \cos\chi + A_T^{(3)} \sin\chi \right], \quad (3.27)$$

where

$$A_C^{(3)}(q^2) = \frac{V_1^{0T}}{(A_L + A_T)}. \quad (3.28)$$

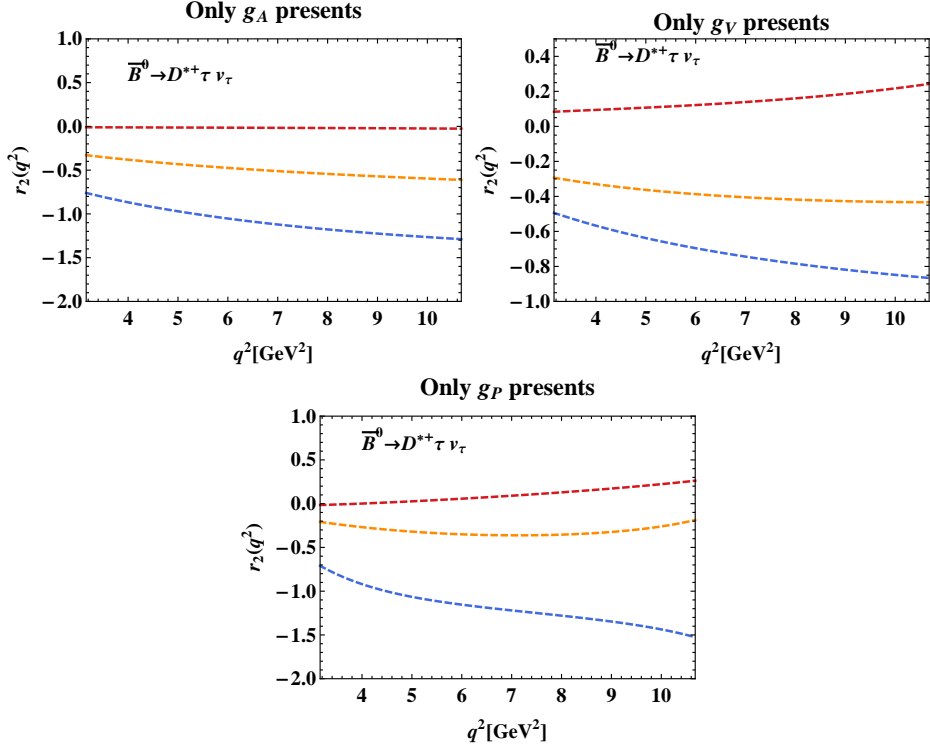


Figure 9: The figures show $r_2(q^2)$ for the decay $\bar{B}^0 \rightarrow D^{*+} \tau \nu_\tau$ in the scenario where only the g_A , only the g_V and only the g_P couplings are present. The values of red and blue dashed lines are given in the figure caption of Fig.8.

Here $A_T^{(3)}$ is a TP, and is discussed separately below. For the conjugate mode

$$\bar{A}_C^{(3)}(q^2) = \frac{\bar{V}_1^{0T}}{(\bar{A}_L + \bar{A}_T)}. \quad (3.29)$$

In the absence of direct CP violation $\bar{A}_C^{(3)} = A_C^{(3)}$. We define the average $A_C^{(3)}(q^2)$ as

$$\langle A_C^{(3)}(q^2) \rangle = \frac{1}{2} \left(A_C^{(3)}(q^2) + \bar{A}_C^{(3)}(q^2) \right). \quad (3.30)$$

The angular coefficient V_1^{0T} depends only on the g_A coupling. Due to cancellations of the NP contributions, $\langle A_C^{(3)}(q^2) \rangle$ behaves similar to its SM prediction when only the g_A coupling is present. The SM prediction of $\langle A_C^{(3)}(q^2) \rangle$ is shown in the green band of Fig. 10(left panel). $\langle A_C^{(3)}(q^2) \rangle$ is not sensitive to the new g_V coupling. As shown in Fig. 10(left panel), $\langle A_C^{(3)}(q^2) \rangle$ is suppressed relative to the SM by the new g_P coupling. The magnitude of the ratio $r_3(q^2) = [A_C^{(3)}(q^2)]^{SM+NP}/[A_C^{(3)}(q^2)]^{SM} - 1 = [A_C^{(3)}(q^2)]^{NP}/[A_C^{(3)}(q^2)]^{SM}$ can reach values $\gtrsim 30\%$ at low q^2 as shown in Fig. 10(right panel).

3.5 CP-violating triple-product asymmetries

In this subsection, we consider the TPs in the decays $\bar{B} \rightarrow D^*(\rightarrow D\pi)l^-\bar{\nu}_l$ and $B \rightarrow \bar{D}^*(\rightarrow D\pi)l^+\nu_l$. For the decaying \bar{B} meson, the TP is proportional to $(\hat{n}_D \times \hat{n}_l) \cdot \hat{n}_z$

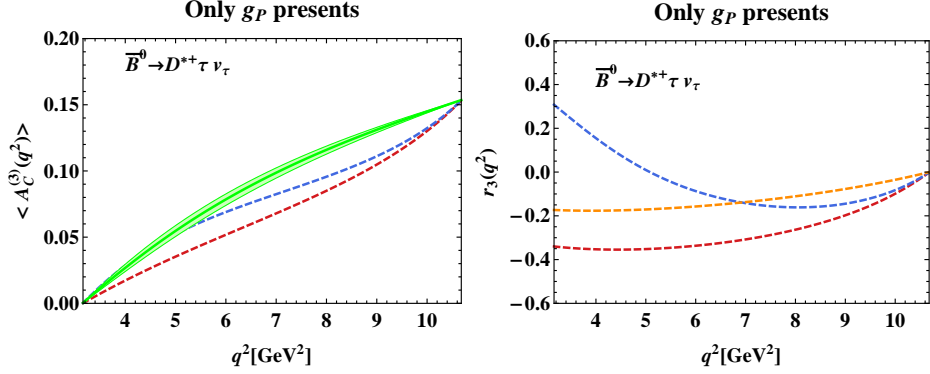


Figure 10: The figure shows $\langle A_C^{(3)}(q^2) \rangle$ and $r_3(q^2)$ for the decay $\bar{B}^0 \rightarrow D^{*+} \tau \nu_\tau$ in the scenario where only the g_P coupling is present. The green band corresponds to the SM prediction and its uncertainties. The red and blue dashed lines correspond to $|g_P|e^{i\phi_{gP}} = 2.03e^{i2.67}$ and $|g_P|e^{i\phi_{gP}} = 3.08e^{i0.63}$, respectively. The values of the couplings are chosen to show the maximum and minimum deviations from the SM expectations.

in its rest frame, where the unit vectors are given in terms of the momenta of the final-state particles as [39]

$$\hat{n}_D = \frac{\hat{p}_D \times \hat{p}_\pi}{|\hat{p}_D \times \hat{p}_\pi|}, \quad \hat{n}_z = \frac{\hat{p}_D + \hat{p}_\pi}{|\hat{p}_D + \hat{p}_\pi|} = \{0, 0, 1\}, \quad \hat{n}_l = \frac{\hat{p}_{l^-} \times \hat{p}_{\bar{\nu}_\tau}}{|\hat{p}_{l^-} \times \hat{p}_{\bar{\nu}_\tau}|}. \quad (3.31)$$

The vectors \hat{n}_D and \hat{n}_l are perpendicular to the decay planes of the D^* and the virtual vector boson. In terms of the azimuthal angle χ , one gets

$$\cos \chi = \hat{n}_D \cdot \hat{n}_l, \quad \sin \chi = (\hat{n}_D \times \hat{n}_l) \cdot \hat{n}_z, \quad (3.32)$$

and hence the quantities that are coefficients of $\sin \chi$ (or of $\sin 2\chi = 2 \sin \chi \cos \chi$) are the TPs.

As noted above, while the angular distribution for the \bar{B} decay involves χ , for B it involves $-\chi$. The TPs in the SM vanish to a very good approximation, as we have mentioned earlier, and this result is free from any hadronic uncertainties. However, with NP the TPs are not zero in general for complex NP couplings. The non-zero TPs now depend on the form factors and suffer from the hadronic uncertainties coming from the form factors. In our calculation for the TPs we have used the inputs for the form factors at their central values. The hadronic uncertainties in the TPs predictions are included in the range of the various NP couplings.

3.5.1 $A_T^{(1)}$

The first TP is $A_T^{(1)}$, introduced above in Eq. (3.17). One can find $A_T^{(1)}$ and $\bar{A}_T^{(1)}$ as

$$A_T^{(1)}(q^2) = \frac{4V_5^T}{3(A_L + A_T)}, \quad \bar{A}_T^{(1)}(q^2) = -\frac{4\bar{V}_5^T}{3(\bar{A}_L + \bar{A}_T)}. \quad (3.33)$$

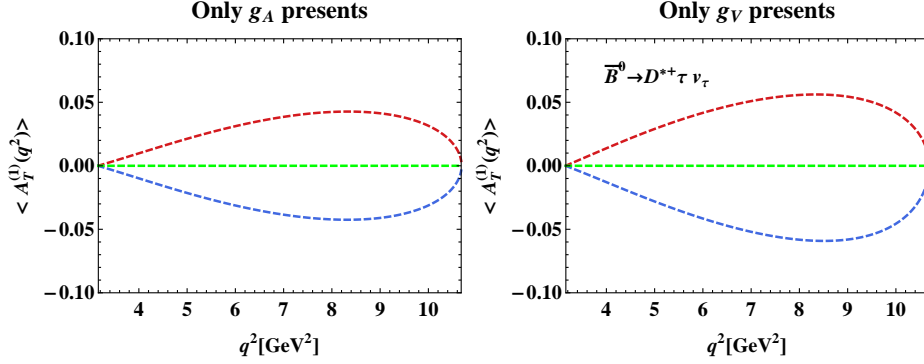


Figure 11: The left and right panels of the figure show $\langle A_T^{(1)}(q^2) \rangle$ for the decay $\bar{B} \rightarrow D^{*+} \tau^- \bar{\nu}_\tau$ in the scenario where only the g_A and only the g_V couplings are present. The green dashed line corresponds to the SM prediction. The red and blue dashed lines correspond to $|g_A|e^{i\phi_{g_A}} = 1.3e^{i0.92}$ and $|g_A|e^{i\phi_{g_A}} = 1.56e^{-i0.74}$ respectively, in the left panel, and $|g_V|e^{i\phi_{g_V}} = 1.73e^{i2.34}$ and $|g_V|e^{i\phi_{g_V}} = 1.75e^{-i2.25}$ in the right panel. The values of the couplings are chosen to show the maximum and minimum deviations from the SM expectations.

In the absence of direct CP violation $\bar{A}_T^{(1)} = A_T^{(1)}$. We observe that $A_T^{(1)}$ depends on both the g_A and the g_V couplings and not on the g_P coupling. The CP-violating triple-product asymmetry is

$$\langle A_T^{(1)}(q^2) \rangle = \frac{1}{2} \left(A_T^{(1)}(q^2) + \bar{A}_T^{(1)}(q^2) \right). \quad (3.34)$$

Fig. 11 shows $\langle A_T^{(1)}(q^2) \rangle$ for $\bar{B} \rightarrow D^{*+} \tau^- \bar{\nu}_\tau$ in the presence of only the g_A and only the g_V couplings. We make the following observations:

- If only the g_A coupling is present, the magnitude of $\langle A_T^{(1)}(q^2) \rangle$ can be enhanced up to 4% at $q^2 \approx 8.0 \text{ GeV}^2$. It vanishes at the end points as the amplitude \mathcal{A}_\perp diminishes. $\langle A_T^{(1)}(q^2) \rangle$ can be either positive or negative. It may or may not have non-SM zero crossing points.
- If only the g_V couplings is present, the magnitude of $\langle A_T^{(1)}(q^2) \rangle$ can be enhanced up to 5% at $q^2 \approx 8.0 \text{ GeV}^2$. The behavior of $\langle A_T^{(1)}(q^2) \rangle$ is similar to the above case.

3.5.2 $A_T^{(2)}$

The second TP is $A_T^{(2)}$, introduced above in Eq. (3.22). $A_T^{(2)}$ and $\bar{A}_T^{(2)}$ are given by

$$A_T^{(2)}(q^2) = \frac{V_3^{0T}}{(A_L + A_T)}, \quad \bar{A}_T^{(2)} = \frac{\bar{V}_3^{0T}}{(\bar{A}_L + \bar{A}_T)}. \quad (3.35)$$

We observe that $A_T^{(2)}(q^2)$ depends on all the three new couplings g_A , g_V , and g_P . This TP is proportional to the lepton mass and so is very small when the lepton is the electron or the muon. The CP-violating triple-product asymmetry is

$$\langle A_T^{(2)}(q^2) \rangle = \frac{1}{2} \left(A_T^{(2)}(q^2) - \bar{A}_T^{(2)}(q^2) \right). \quad (3.36)$$

Fig. 12 shows $\langle A_T^{(2)}(q^2) \rangle$ for $\bar{B} \rightarrow D^{*+} \tau^- \bar{\nu}_\tau$ in the presence of only the g_A , only the g_V and only the g_P couplings. We make the following observations

- If only the g_A coupling is present, the magnitude of $\langle A_T^{(2)}(q^2) \rangle$ can go up to 10% at low q^2 and this TP vanishes at the end points. It can have either sign at both low and high q^2 . Also $\langle A_T^{(2)} \rangle$ may or may not have non-SM zero crossing.
- If only the g_V coupling is present, the magnitude of $\langle A_T^{(2)}(q^2) \rangle$ can reach up to 10% at low q^2 . The behavior of $\langle A_T^{(2)}(q^2) \rangle$ is similar to the one when only the g_A coupling is present.
- If only the g_P coupling is present, the asymmetry prediction is similar to the other two cases.

3.5.3 $A_T^{(3)}$

The third TP is $A_T^{(3)}$, introduced above in Eq. (3.27). $A_T^{(3)}$ and $\bar{A}_T^{(3)}$ are given by

$$A_T^{(3)}(q^2) = \frac{V_4^{0T}}{(A_L + A_T)}, \quad \bar{A}_T^{(3)} = -\frac{\bar{V}_4^{0T}}{(\bar{A}_L + \bar{A}_T)}. \quad (3.37)$$

We observe that $A_T^{(3)}$ depends on both the new couplings g_A and g_V but does not depend on g_P . The CP-violating triple-product asymmetry is

$$\langle A_T^{(3)}(q^2) \rangle = \frac{1}{2} \left(A_T^{(3)}(q^2) + \bar{A}_T^{(3)}(q^2) \right). \quad (3.38)$$

Fig. 13 shows $\langle A_T^{(3)} \rangle$ for $\bar{B} \rightarrow D^{*+} \tau^- \bar{\nu}_\tau$ in the presence of only the g_A and only the g_V couplings. We make the following observations:

- If only the g_A coupling is present, the magnitude of $\langle A_T^{(3)}(q^2) \rangle$ can be enhanced up to 4% at $q^2 \approx 8.0 \text{ GeV}^2$ and it vanishes at the end points. $\langle A_T^{(3)}(q^2) \rangle$ can have either sign at both low and high q^2 . Also it may or may not have a non-SM zero crossing.
- If only the g_V coupling is present, the magnitude of $\langle A_T^{(3)}(q^2) \rangle$ can be enhanced up to 5% at $q^2 \approx 8.0 \text{ GeV}^2$. The behavior of $\langle A_T^{(3)}(q^2) \rangle$ is similar to the case above.

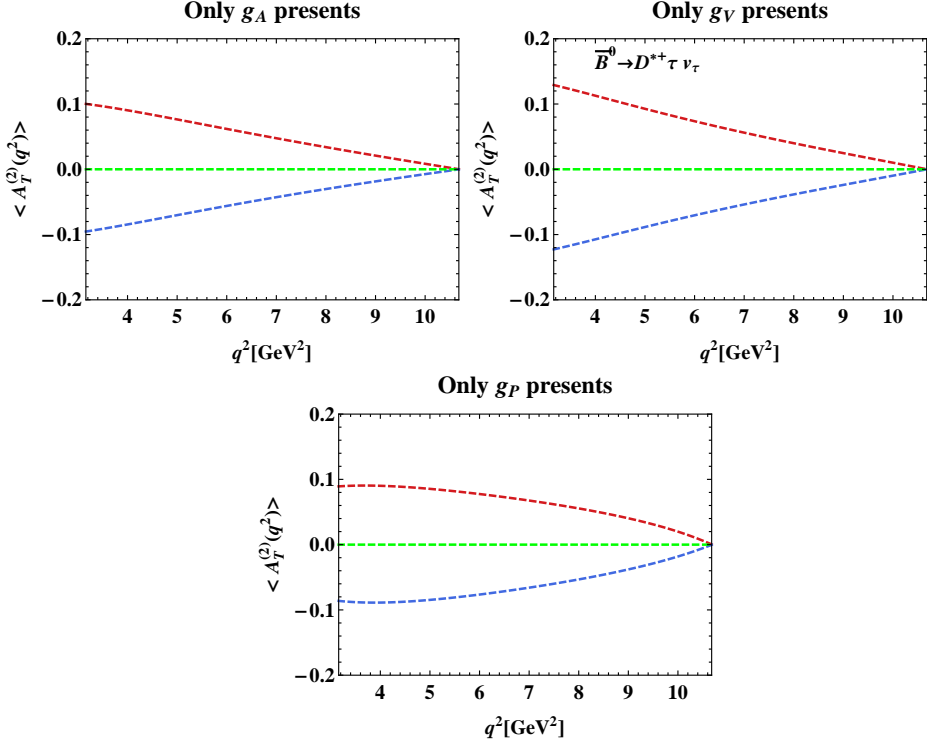


Figure 12: The figures show $\langle A_T^{(2)}(q^2) \rangle$ for the decay $\bar{B}^0 \rightarrow D^{*+} \tau \nu_\tau$ in the scenario where only the g_A , only the g_V , and only the g_P couplings are present. The green dashed line corresponds to the SM prediction. The red and blue dashed lines correspond to $|g_A|e^{i\phi_{g_A}} = 1.32e^{-i0.88}$ and $|g_A|e^{i\phi_{g_A}} = 0.92e^{i0.27}$ respectively, in the upper-left panel, $|g_V|e^{i\phi_{g_V}} = 1.51e^{-i2.11}$ and $|g_V|e^{i\phi_{g_V}} = 1.51e^{i2.08}$ in the upper-right panel, and $|g_P|e^{i\phi_{g_P}} = 3.57e^{-i1.14}$ and $|g_P|e^{i\phi_{g_P}} = 2.86e^{i0.96}$ in the lower panel. The values of the couplings are chosen to show the maximum and minimum deviations from the SM expectations.

3.6 Correlations between R_{D^*} and q^2 -integrated TP asymmetries

As we discussed in the previous section, the three CP-violating TP asymmetries $A_T^{(1,2,3)}(q^2)$ are sensitive to the new g_A and g_V couplings. It is useful to study the correlations between the q^2 -integrated TP asymmetries $\langle A_T^{(1,2,3)} \rangle$ and R_{D^*} in the presence of these new couplings. Fig. 14 shows the correlation between $\langle A_T^{(1,2,3)} \rangle$ and R_{D^*} in the presence of only the g_A and only the g_V couplings. The orange(blue) color scatter plots correspond to only the $g_A(g_V)$ couplings. Here we have varied the magnitude of $g_A(g_V)$ between (0, 2.5) and its phase between $(-\pi, \pi)$. All other theoretical inputs are kept at their central values. The vertical bands correspond to the measured R_{D^*} in Eq.(1.1) with $\pm 1\sigma$ (green) and $\pm 2\sigma$ (yellow) errors. We make the following observations for the measured R_{D^*} within $\pm 2\sigma$ errors :

- If only the g_A coupling is present, the magnitude of $\langle A_T^{(1,3)} \rangle$ can reach up to 3% while $\langle A_T^{(2)} \rangle$ can be up to 5%. All these asymmetries can have either sign.

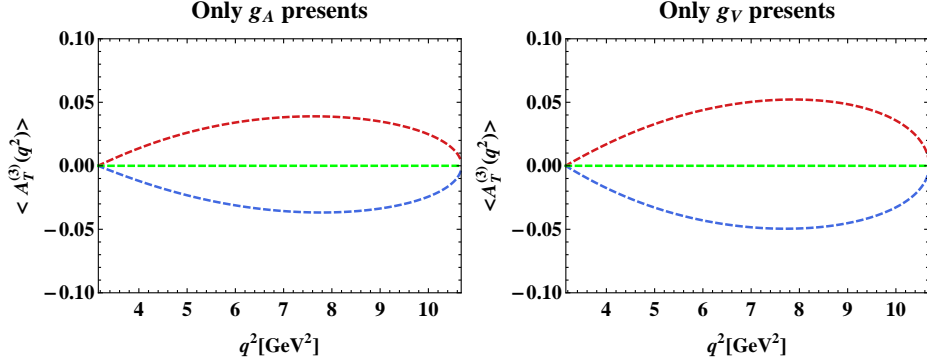


Figure 13: The left and right panels of the figure show $\langle A_T^{(3)}(q^2) \rangle$ for the decay $\bar{B} \rightarrow D^{*+} \tau^- \bar{\nu}_\tau$ in the scenario where only the g_A and only the g_V couplings are present. The green dashed line corresponds to the SM prediction. The red and blue dashed lines correspond to $|g_A|e^{i\phi_{g_A}} = 1.44e^{-i0.82}$ and $|g_A|e^{i\phi_{g_A}} = 1.66e^{-i0.74}$ respectively, in the left panel, and $|g_V|e^{i\phi_{g_V}} = 1.75e^{-i2.25}$ and $|g_V|e^{i\phi_{g_V}} = 1.5e^{i2.1}$ in the right panel. The values of the couplings are chosen to show the maximum and minimum deviations from the SM expectations.

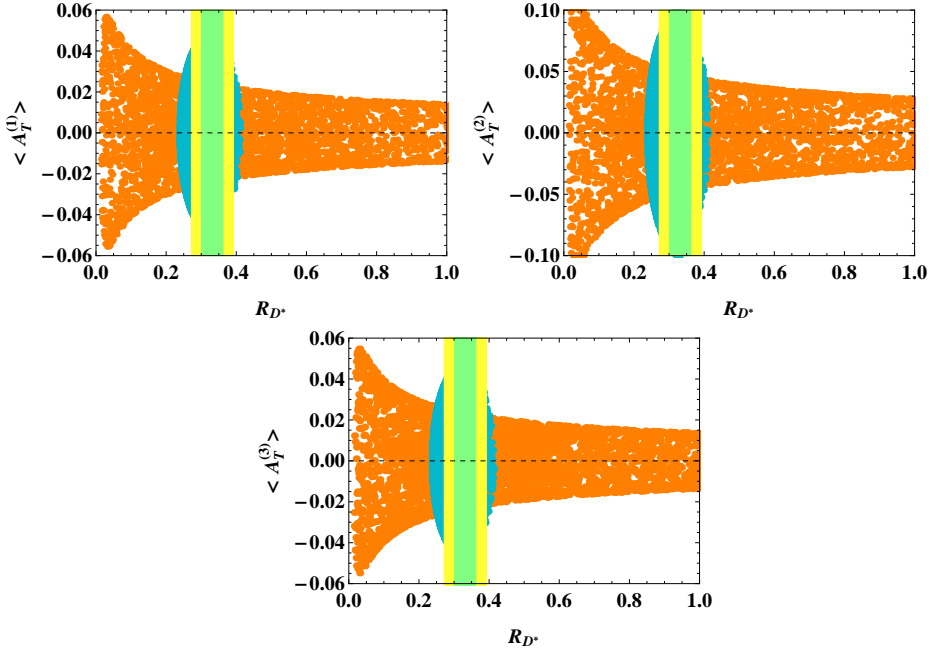


Figure 14: The figure shows the correlation between $\langle A_T^{(1,2,3)} \rangle$ and R_{D^*} in the presence of only the g_A and only the g_V couplings. See the text for details.

- If only the g_V coupling is present, the magnitude of $\langle A_T^{(1,3)} \rangle$ can reach up to 5% while $\langle A_T^{(2)} \rangle$ can reach up to 10%. All these asymmetries can have either sign.

The new g_P coupling can only significantly affect $\langle A_T^{(2)} \rangle$. As shown in the pink scatter plot in Fig. 15, $\langle A_T^{(2)} \rangle$ can reach up to 6% for the measured R_{D^*} within $\pm 2\sigma$

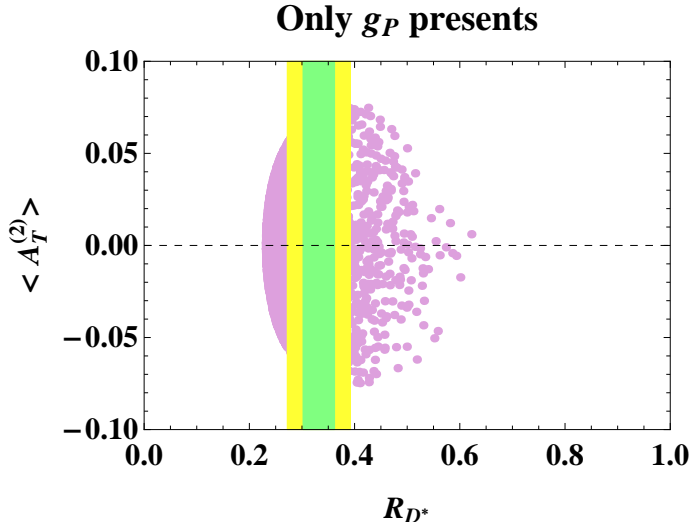


Figure 15: The figure show the correlation between $\langle A_T^{(1,2,3)} \rangle$ and R_{D^*} in the presence of only the g_P coupling.

errors in this scenario. This asymmetry can have either sign.

4. Discussion and Summary

We presented the full three angle and q^2 distribution for $\bar{B} \rightarrow D^* \ell^- \bar{\nu}_\ell$. We focused on the decay $\bar{B} \rightarrow D^{*+} \tau^- \bar{\nu}_\tau$, since the new experimental results are not consistent with SM predictions. We extended the work of Ref. [17] by considering additional observables from the angular distribution. Particular attention was paid to the CP violating triple product asymmetries. It was argued that in the SM these asymmetries vanish, to a very good approximation, and so non-zero measurements of these asymmetries would be smoking gun signals for new physics. Of the three triple product asymmetries two are sensitive to only vector and axial vector new physics. Hence the triple product asymmetries are not only sensitive to new physics but also can probe the nature of new physics. Our results are summarized in Table 2, for the cases where the NP has only one type of Lorentz structure: $g_A = V_R - V_L$, $g_V = V_R + V_L$, or $g_P = S_R - S_L$.

Acknowledgements

This work was supported in part by the National Science Foundation under Grant No. NSF PHY-1068052. AD thanks A. Soffer, M. Roney and Manuel Franco Sevilla for useful discussions.

Observable	SM	Only new $g_A = V_R - V_L$	Only new $g_V = V_R + V_L$	Only new $g_P = S_R - S_L$
DBR		• Significant E	• No effect	• Significant E
$R_{D^*}(q^2)$	• $0 \rightarrow 0.55$ (low \rightarrow high q^2)	• Significant E at high q^2	• No effect	• Significant E at $q^2 \approx 7.5\text{GeV}^2$
$f_L(q^2)$	• $0.75 \rightarrow 0.35$ (low \rightarrow high q^2)	• No effect	• No effect	• Marginal E
$A_{FB}(q^2)$	• ZC ≈ 5.64 GeV^2	• Significant S at low q^2 • ZC may / may not exist	• Significant S at low q^2 • ZC may / may not exist	• Significant E/ S at low q^2 • ZC may / may not exist
$A_C^{(1)}(q^2)$	• $0.0 \rightarrow -0.2$ (low \rightarrow high q^2) • No ZC	• No effect	• No effect	• Marginal E at $q^2 \approx 8.0\text{GeV}^2$
$A_C^{(2)}(q^2)$	• $0.3 \rightarrow 0.0$ (low \rightarrow high q^2) • No ZC	• Significant S • ZC may / may not exist	• Significant S • ZC may / may not exist	• Significant S • ZC may / may not exist
$A_C^{(3)}(q^2)$	• $0.0 \rightarrow 0.15$ (low \rightarrow high q^2) • No ZC	• No effect	• No effect	• Marginal S
$A_T^{(1)}(q^2)$		• Significant E/ S at $q^2 \approx 8.0\text{GeV}^2$ • ZC may / may not exist	• Significant E/ S at $q^2 \approx 8.0\text{GeV}^2$ • ZC may / may not exist	• No effect
$A_T^{(2)}(q^2)$		• Significant E/ S at low q^2 • ZC may / may not exist	• Significant E/ S at low q^2 • ZC may / may not exist	• Significant E/ S at low q^2 • ZC may / may not exist
$A_T^{(3)}(q^2)$		• Significant E/ S at $q^2 \approx 8.0\text{GeV}^2$ • ZC may / may not exist	• Significant E/ S at $q^2 \approx 8.0\text{GeV}^2$ • ZC may / may not exist	• No effect

Table 2: The effect of NP couplings on observables. E: enhancement, S: suppression, ZC: zero crossing.

A. Details of the $\bar{B} \rightarrow D^* \tau^- \bar{\nu}_\tau$ angular analysis

A.1 kinematics

In the B rest frame, the co-ordinates are chosen such that the D^* meson is moving along the positive z -axis, whereas the virtual gauge boson is moving along the negative z -axis. The four-momenta of the B and D^* mesons, and the virtual gauge boson are

$$p_B = (m_B, 0, 0, 0), \quad p_{D^*} = (E_{D^*}, 0, 0, |p_{D^*}|), \quad q = (q_0, 0, 0, -|p_{D^*}|), \quad (\text{A.1})$$

where $E_{D^*} = (m_B^2 + m_{D^*}^2 - q^2)/2m_B$, $|p_{D^*}| = \lambda^{1/2}(m_B^2, m_{D^*}^2, q^2)/2m_B$, and $q_0 = (m_B^2 - m_{D^*}^2 + q^2)/2m_B$. Further, one chooses the polarization vector of the D^* meson as

$$\epsilon(0) = \frac{1}{m_{D^*}}(|p_{D^*}|, 0, 0, E_{D^*}), \quad \epsilon(\pm) = \mp \frac{1}{\sqrt{2}}(0, 1, \pm i, 0). \quad (\text{A.2})$$

In this frame, we choose the polarization vector of the virtual gauge boson $\bar{\epsilon}$, which can be, longitudinal ($m = 0$), transverse ($m = \pm$), or timelike ($m = t$):

$$\begin{aligned} \bar{\epsilon}(0) &= \frac{1}{\sqrt{q^2}}(|p_{D^*}|, 0, 0, -q_0), \quad \bar{\epsilon}(\pm) = \frac{1}{\sqrt{2}}(0, \pm 1, -i, 0), \\ \bar{\epsilon}(t) &= \frac{q^\mu}{\sqrt{q^2}} = \frac{1}{\sqrt{q^2}}(q_0, 0, 0, -|p_{D^*}|), \end{aligned} \quad (\text{A.3})$$

The leptonic tensor is evaluated in the q^2 rest frame. In this frame, we choose the transverse components of the helicity basis $\bar{\epsilon}$ to remain the same and other two components are taken as

$$\bar{\epsilon}(0) = (0, 0, 0, -1), \quad \bar{\epsilon}(t) = (1, 0, 0, 0). \quad (\text{A.4})$$

Let θ_l be the angle between the three-momenta of D^* meson and the charged lepton in the q^2 rest frame, and χ be the opening angle between the two decay planes. We define the momenta of the lepton and anti-neutrino pairs as

$$\begin{aligned} p_l^\mu &= (E_l, pl \sin \theta_l \cos \chi, pl \sin \theta_l \sin \chi, -pl \cos \theta_l), \\ p_\nu^\mu &= (p_l, -pl \sin \theta_l \cos \chi, -pl \sin \theta_l \sin \chi, pl \cos \theta_l), \end{aligned} \quad (\text{A.5})$$

where the lepton energy $E_l = (q^2 + m_l^2)/2\sqrt{q^2}$ and the magnitude of its three-momenta is $p_l = (q^2 - m_l^2)/2\sqrt{q^2}$.

A.2 Form Factors

The relevant form factors for the $B \rightarrow D^*$ matrix elements of the vector $V_\mu = \bar{c}\gamma^\mu b$ and axial-vector $A_\mu = \bar{c}\gamma^\mu\gamma_5 b$ currents are defined as [41]

$$\begin{aligned}\langle D^*(p_{D^*}, \epsilon^*) | V_\mu | \bar{B}(p_B) \rangle &= \frac{2iV(q^2)}{m_B + m_{D^*}} \epsilon_{\mu\nu\rho\sigma} \epsilon^{*\nu} p_{D^*}^\rho p_B^\sigma, \\ \langle D^*(p_{D^*}, \epsilon^*) | A_\mu | \bar{B}(p_B) \rangle &= 2m_{D^*} A_0(q^2) \frac{\epsilon^* \cdot q}{q^2} q_\mu + (m_B + m_{D^*}) A_1(q^2) \left[\epsilon_\mu^* - \frac{\epsilon^* \cdot q}{q^2} q_\mu \right] \\ &\quad - A_2(q^2) \frac{\epsilon^* \cdot q}{(m_B + m_{D^*})} \left[(p_B + p_{D^*})_\mu - \frac{m_B^2 - m_{D^*}^2}{q^2} q_\mu \right].\end{aligned}\quad (\text{A.6})$$

In addition, from Eq. (A.6) one can show that the $B \rightarrow D^*$ matrix element for the scalar current vanishes and for the pseudoscalar current reduces to

$$\langle D^*(p_{D^*}, \epsilon^*) | \bar{c}\gamma_5 b | \bar{B}(p_B) \rangle = -\frac{2m_{D^*} A_0(q^2)}{m_b(\mu) + m_c(\mu)} \epsilon^* \cdot q. \quad (\text{A.7})$$

B. Form factors in the Heavy Quark Effective Theory

In the heavy quark limit for the b, c quarks ($m_{b,c} \gg \Lambda_{QCD}$), both charm and the bottom quark in the hadronic current have to be replaced by static quarks $h_{v',c}$ and $h_{v,b}$, where $v_B^\mu = p_B/m_B$ and $v_{D^*}^\mu = p_{D^*}/m_{D^*}$ are the four-velocities of the B and D^* mesons, respectively. The $b \rightarrow c$ transition can be studied in the heavy quark effective theory (HQET). In this effective theory, the matrix elements of the vector and axial vector currents, V_μ and A_μ , between bottom and charm mesons [42] are defined as

$$\begin{aligned}\langle D(v') | V_\mu | B(v) \rangle &= \sqrt{m_B m_D} \left[h_+(w) (v + v')_\mu + h_-(w) (v - v')_\mu \right], \\ \langle D^*(v', \epsilon') | V_\mu | B(v) \rangle &= i\sqrt{m_B m_{D^*}} h_V(w) \epsilon_{\mu\nu\alpha\beta} \epsilon'^{\nu} v'^\alpha v^\beta, \\ \langle D^*(v', \epsilon') | A_\mu | B(v) \rangle &= \sqrt{m_B m_{D^*}} \left[h_{A_1}(w) (w + 1) \epsilon_\mu^* - h_{A_2}(w) \epsilon'^* \cdot v v_\mu \right. \\ &\quad \left. - h_{A_3}(w) \epsilon'^* \cdot v v'_\mu \right],\end{aligned}\quad (\text{B.1})$$

where the kinematical variable $w = v_B \cdot v_{D^*} = (m_B^2 + m_{D^*}^2 - q^2)/2m_B m_{D^*}$.

The form factors $h_{A_i}(w)$ are related to the form factors in Eq. (A.6) [13, 32, 35] in the following way,

$$\begin{aligned}A_1(q^2) &= R_{D^*} \frac{w + 1}{2} h_{A_1}(w), \quad A_0(q^2) = \frac{R_0(w)}{R_{D^*}} h_{A_1}(w), \\ A_2(q^2) &= \frac{R_2(w)}{R_{D^*}} h_{A_1}(w), \quad V(q^2) = \frac{R_1(w)}{R_{D^*}} h_{A_1}(w),\end{aligned}\quad (\text{B.2})$$

where $R_{D^*} = 2\sqrt{m_B m_D^*}/(m_B + m_D^*)$. The w dependence of the form factors can be found in [13, 32] and the summary of the results are

$$\begin{aligned} h_{A_1}(w) &= h_{A_1}(1) \left[1 - 8\rho^2 z + (53\rho^2 - 15)z^2 - (231\rho^2 - 91)z^3 \right], \\ R_1(w) &= R_1(1) - 0.12(w - 1) + 0.05(w - 1)^2, \\ R_2(w) &= R_2(1) + 0.11(w - 1) - 0.06(w - 1)^2, \\ R_0(w) &= R_0(1) - 0.11(w - 1) + 0.01(w - 1)^2, \end{aligned} \quad (\text{B.3})$$

where $z = (\sqrt{w+1} - \sqrt{2})/(\sqrt{w+1} + \sqrt{2})$. The numerical values of the free parameters ρ^2 , $h_{A_1}(1)$, $R_1(1)$ and $R_2(1)$ are taken from [35],

$$\begin{aligned} h_{A_1}(1)|V_{cb}| &= (34.6 \pm 0.2 \pm 1.0) \times 10^{-3}, \\ \rho^2 &= 1.214 \pm 0.034 \pm 0.009, \\ R_1(1) &= 1.401 \pm 0.034 \pm 0.018, \\ R_2(1) &= 0.864 \pm 0.024 \pm 0.008, \end{aligned} \quad (\text{B.4})$$

and $R_0(1) = 1.14$ is taken from [13]. In the numerical analysis, we allow 10% uncertainties in the $R_0(1)$ value to account for higher-order corrections.

In the HQET, the transversity amplitudes of Eq. (2.5) become

$$\begin{aligned} \mathcal{A}_0 &= \frac{m_B(1 - r_*)(w + 1)\sqrt{r_*}}{\sqrt{(1 + r_*^2 - 2r_*w)}} h_{A_1}(w) \left[1 + \frac{(w - 1)(1 - R_2(w))}{(1 - r_*)} \right] (1 - g_A), \\ \mathcal{A}_\parallel &= m_B \sqrt{2r_*(w + 1)} h_{A_1}(w) (1 - g_A), \\ \mathcal{A}_\perp &= -m_B \sqrt{2r_*(w^2 - 1)} h_{A_1}(w) R_1(w) (1 + g_V), \\ \mathcal{A}_{tP} &= m_B (1 + r_*) \sqrt{\frac{r_*(w^2 - 1)}{(1 + r_*^2 - 2r_*w)}} h_{A_1}(w) R_0(w) \left[(1 - g_A) - \frac{m_B^2(1 + r_*^2 - 2r_*w)}{m_l(m_b(\mu) + m_c(\mu))} g_P \right], \end{aligned} \quad (\text{B.5})$$

where $r_* = m_{D^*}/m_B$, and

$$\mathcal{A}_{tP} = \left(\mathcal{A}_t + \frac{\sqrt{q^2}}{m_\tau} \mathcal{A}_P \right). \quad (\text{B.6})$$

B.1 Angular coefficients

The expressions for the twelve angular coefficients V_i^λ in the $B \rightarrow D^*(\rightarrow D\pi)l^-\bar{\nu}_l$ angular distribution are summarized according to the D^* helicity combinations $\lambda_1\lambda_2$.

The longitudinal V^0 's ($\lambda_1\lambda_2 = 00$) are given by

$$\begin{aligned} V_1^0 &= 2 \left(1 + \frac{m_l^2}{q^2} \right) |A_0|^2 + \frac{4m_l^2}{q^2} |A_{tP}|^2, \\ V_2^0 &= -2 \left(1 - \frac{m_l^2}{q^2} \right) |A_0|^2, \\ V_3^0 &= -8 \frac{m_l^2}{q^2} \text{Re}[A_{tP}A_0^*]. \end{aligned} \quad (\text{B.7})$$

The transverse V^T 's ($\lambda_1\lambda_2 = ++, --, +-, -+$) are given by

$$\begin{aligned}
V_1^T &= \frac{1}{2} \left(3 + \frac{m_l^2}{q^2} \right) \left(|A_{\parallel}|^2 + |A_{\perp}|^2 \right) , \\
V_2^T &= \frac{1}{2} \left(1 - \frac{m_l^2}{q^2} \right) \left(|A_{\parallel}|^2 + |A_{\perp}|^2 \right) , \\
V_3^T &= -4 \text{Re}[A_{\parallel} A_{\perp}^*] , \\
V_4^T &= - \left(1 - \frac{m_l^2}{q^2} \right) \left(|A_{\parallel}|^2 - |A_{\perp}|^2 \right) , \\
V_5^T &= \left(1 - \frac{m_l^2}{q^2} \right) \text{Im}[A_{\parallel} A_{\perp}^*] .
\end{aligned} \tag{B.8}$$

The mixed V^{0T} 's ($\lambda_1\lambda_2 = 0\pm, \pm 0$) are given by

$$\begin{aligned}
V_1^{0T} &= \sqrt{2} \left(1 - \frac{m_l^2}{q^2} \right) \text{Re}[A_{\parallel} A_0^*] , \\
V_2^{0T} &= 2\sqrt{2} \text{Re} \left[-A_{\perp} A_0^* + \frac{m_l^2}{q^2} A_{\parallel} A_{tP}^* \right] , \\
V_3^{0T} &= 2\sqrt{2} \text{Im} \left[-A_{\parallel} A_0^* + \frac{m_l^2}{q^2} A_{\perp} A_{tP}^* \right] , \\
V_4^{0T} &= \sqrt{2} \left(1 - \frac{m_l^2}{q^2} \right) \text{Im}[A_{\perp} A_0^*] .
\end{aligned} \tag{B.9}$$

References

- [1] A. Filipuzzi, J. Portoles and M. Gonzalez-Alonso, arXiv:1203.2092 [hep-ph].
- [2] J. P. Lees *et al.* [BABAR Collaboration], Phys. Rev. D **85**, 031102 (2012) [Erratum-ibid. D **85**, 099904 (2012)] [arXiv:1109.1527 [hep-ex]].
- [3] K. Ikado *et al.*, Phys. Rev. Lett. **97**, 251802 (2006) [arXiv:hep-ex/0604018].
- [4] See for example, B. Bhattacharjee, A. Dighe, D. Ghosh and S. Raychaudhuri, Phys. Rev. D **83**, 094026 (2011) [arXiv:1012.1052 [hep-ph]].
- [5] I. Adachi *et al.* [Belle Collaboration], arXiv:1208.4678 [hep-ex].
- [6] J. P. Lees *et al.* [BABAR Collaboration], arXiv:1207.0698 [hep-ex].
- [7] U. Nierste, S. Trine and S. Westhoff, Phys. Rev. D **78**, 015006 (2008) [arXiv:0801.4938 [hep-ph]].
- [8] A. Matyja *et al.* [Belle Collaboration], Phys. Rev. Lett. **99**, 191807 (2007) [arXiv:0706.4429 [hep-ex]].
- [9] B. Aubert *et al.* [BABAR Collaboration], Phys. Rev. Lett. **100**, 021801 (2008) [arXiv:0709.1698 [hep-ex]].

- [10] I. Adachi *et al.* [Belle Collaboration], arXiv:0910.4301 [hep-ex].
- [11] A. Bozek *et al.* [Belle Collaboration], Phys. Rev. D **82**, 072005 (2010) [arXiv:1005.2302 [hep-ex]].
- [12] J. P. Lees *et al.* [BaBar Collaboration], Phys. Rev. Lett. **109**, 101802 (2012) [arXiv:1205.5442 [hep-ex]].
- [13] S. Fajfer, J. F. Kamenik and I. Nisandzic, arXiv:1203.2654 [hep-ph].
- [14] Y. Sakaki and H. Tanaka, arXiv:1205.4908 [hep-ph].
- [15] S. Fajfer, J. F. Kamenik, I. Nisandzic and J. Zupan, Phys. Rev. Lett. **109**, 161801 (2012) [arXiv:1206.1872 [hep-ph]].
- [16] A. Crivellin, C. Greub and A. Kokulu, Phys. Rev. D **86**, 054014 (2012) [arXiv:1206.2634 [hep-ph]].
- [17] A. Datta, M. Duraisamy and D. Ghosh, Phys. Rev. D **86**, 034027 (2012) [arXiv:1206.3760 [hep-ph]].
- [18] D. Becirevic, N. Kosnik and A. Tayduganov, Phys. Lett. B **716**, 208 (2012) [arXiv:1206.4977 [hep-ph]].
- [19] N. G. Deshpande and A. Menon, arXiv:1208.4134 [hep-ph].
- [20] A. Celis, M. Jung, X. -Q. Li and A. Pich, JHEP **1301**, 054 (2013) [arXiv:1210.8443 [hep-ph]].
- [21] D. Choudhury, D. K. Ghosh and A. Kundu, Phys. Rev. D **86**, 114037 (2012) [arXiv:1210.5076 [hep-ph]].
- [22] M. Tanaka and R. Watanabe, arXiv:1212.1878 [hep-ph].
- [23] P. Ko, Y. Omura and C. Yu, arXiv:1212.4607 [hep-ph].
- [24] Y. -Y. Fan, W. -F. Wang and Z. -J. Xiao, arXiv:1301.6246 [hep-ph].
- [25] P. Biancofiore, P. Colangelo and F. De Fazio, arXiv:1302.1042 [hep-ph].
- [26] A. Celis, M. Jung, X. -Q. Li and A. Pich, arXiv:1302.5992 [hep-ph].
- [27] A. Datta and D. London, Int. J. Mod. Phys. A **19**, 2505 (2004) [hep-ph/0303159]; W. Bensalem, A. Datta and D. London, Phys. Rev. D **66**, 094004 (2002) [hep-ph/0208054]; W. Bensalem, A. Datta and D. London, Phys. Lett. B **538**, 309 (2002) [hep-ph/0205009].
- [28] T. Bhattacharya, V. Cirigliano, S. D. Cohen, A. Filipuzzi, M. Gonzalez-Alonso, M. L. Graesser, R. Gupta and H. -W. Lin, Phys. Rev. D **85**, 054512 (2012) [arXiv:1110.6448 [hep-ph]]; C. -H. Chen and C. -Q. Geng, Phys. Rev. D **71**, 077501 (2005) [hep-ph/0503123].

- [29] See for example, A. Rashed, M. Duraisamy and A. Datta, arXiv:1204.2023 [hep-ph]; A. Datta, P. J. O'Donnell, Z. H. Lin, X. Zhang and T. Huang, Phys. Lett. B **483**, 203 (2000) [hep-ph/0001059]. B. Bhattacharjee, S. S. Biswal and D. Ghosh, Phys. Rev. D **83**, 091501 (2011) [arXiv:1102.0545 [hep-ph]].
- [30] See for e.g. A. Datta, Phys. Rev. D **66**, 071702 (2002) [hep-ph/0208016]; A. Datta and P. J. O'Donnell, Phys. Rev. D **72**, 113002 (2005) [hep-ph/0508314]; A. Datta, Phys. Rev. D **74**, 014022 (2006) [hep-ph/0605039]; A. Datta, Phys. Rev. D **78**, 095004 (2008) [arXiv:0807.0795 [hep-ph]]; C. -W. Chiang, A. Datta, M. Duraisamy, D. London, M. Nagashima and A. Szyrkman, JHEP **1004**, 031 (2010) [arXiv:0910.2929 [hep-ph]].
- [31] M. Neubert, Phys. Rept. **245**, 259 (1994) [hep-ph/9306320].
- [32] I. Caprini, L. Lellouch and M. Neubert, Nucl. Phys. B **530**, 153 (1998) [hep-ph/9712417].
- [33] K. Nakamura *et al.* [Particle Data Group Collaboration], J. Phys. G **37**, 075021 (2010).
- [34] D. Asner *et al.* [Heavy Flavor Averaging Group Collaboration], arXiv:1010.1589 [hep-ex].
- [35] W. Dungen *et al.* [Belle Collaboration], Phys. Rev. D **82**, 112007 (2010) [arXiv:1010.5620 [hep-ex]].
- [36] J. D. Richman and P. R. Burchat, Rev. Mod. Phys. **67**, 893 (1995) [hep-ph/9508250].
- [37] J. G. Korner and G. A. Schuler, Z. Phys. C **46**, 93 (1990).
- [38] J. G. Korner and G. A. Schuler, Phys. Lett. B **231** (1989) 306. J. G. Korner and G. A. Schuler,
- [39] A. K. Alok, A. Datta, A. Dighe, M. Duraisamy, D. Ghosh and D. London, JHEP **1111**, 121 (2011) [arXiv:1008.2367 [hep-ph]]; A. K. Alok, A. Datta, A. Dighe, M. Duraisamy, D. Ghosh and D. London, JHEP **1111**, 122 (2011) [arXiv:1103.5344 [hep-ph]].
- [40] J. P. Lees *et al.* [BaBar Collaboration], arXiv:1303.0571 [hep-ex].
- [41] M. Beneke and T. Feldmann, Nucl. Phys. B **592**, 3 (2001) [hep-ph/0008255].
- [42] A. F. Falk and M. Neubert, Phys. Rev. D **47**, 2965 (1993) [hep-ph/9209268].